

BL6B

Infrared Reflection-Absorption Spectroscopy of Alq₃ Thin Film on Silver Surface Using Synchrotron Radiation

Y. Sakurai¹, S. Kimura^{1,2}, K. Seki³¹UVSOR Facility, Institute for Molecular Science, Okazaki 444-8585, Japan²Department of Structural Molecular Science, The Graduate University for Advanced Studies, Okazaki 444-8585, Japan³Department of Chemistry, Graduate School of Science, Nagoya University, Furo-cho, Chikusa-ku, Nagoya 464-8602, Japan

Recently, organic semiconductors are attracting attention because of possible applications to electronic devices such as organic light emitting diodes (OLEDs). In OLEDs, tris(8-hydroxyquinoline) aluminum (Alq₃) is most widely used as the electron transport/light emitting material [1]. Alq₃ has two possible geometrical isomers of meridional (C₁ symmetry) and facial (C₃ symmetry) forms. In the meridional isomer, the three ligands around the central Al atom are not equivalent (Fig. 1(a)), while they are equivalent in the facial isomer (Fig. 1(b)). It has been reported that the meridional isomer is dominant in evaporated films [2]. However, in the case of Alq₃ molecules adsorbed directly on an Al surface, the facial isomer is predicted to be more stable than the meridional one by a theoretical investigation [3]. Since the facial isomer generally acts as an electron trap in amorphous film [4], this isomer may become an obstacle for the charge transport in the device [3,4]. Thus it is important to find whether facial isomer exists at the interface between the metal and the Alq₃ film or not.

Vibrational spectroscopy such as infrared (IR) spectroscopy is suitable technique for distinguishing these isomers. There is already an IR spectroscopic

study of the Alq₃ isomers by Cölle et al. using the facial isomer isolated in the pure form [5]. For the vibrational modes within the ligands observed in the wavenumber region above 700 cm⁻¹, the differences of the spectra between isomers appear only in the width of the absorption peaks. On the other hand, significant differences appear in the stretching modes around the central Al atom, namely, Al-N and Al-O stretching modes in the wavenumber region below 600 cm⁻¹. Therefore these modes become good probes to distinguish the isomers. In this study, we examined whether the facial isomer exists at the interface between the Ag and the Alq₃ film or not by infrared reflection-absorption spectroscopy (IRAS) using a synchrotron radiation (SR) light source. Use of highly brilliant infrared synchrotron radiation (IRSR) source enables us to obtain IRAS spectra in the low wavenumber region, which cannot be covered by conventional IRAS system using globar light source because of its low brilliance.

The SR-IRAS experiments were performed at an infrared-to-terahertz beamline BL6B of UVSOR-II. SR-IRAS system consists of an ultrahigh vacuum (UHV) chamber with evaporators (for Ag and Alq₃), focusing optics and a detector. Horizontally polarized parallel IRSR from a Michelson interferometer (Bruker IFS66v) is guided to an off-axis parabolic mirror with the focal length f of 152.4 mm to be focused on the sample surface with the incident angle of 80° relative to the surface normal. The reflected light is collected by the second off-axis parabolic mirror ($f=152.4$ mm) and guided to the third off-axis parabolic mirror ($f=101.6$ mm) to be focused on the detector. The UHV chamber is separated from the low vacuum of the focusing and collecting optics chambers by KRS-5 windows. The base pressure of the UHV chamber was below 5×10^{-7} Pa.

The Ag surface was prepared by vacuum evaporation on Si substrates (20 x 7 mm²) using a Knudsen cell. Deposition of Alq₃, which was supplied by Nippon Steel Chemical Co., Ltd., was performed using a glass crucible coiled with a tungsten wire heater. The Ag surface was kept at room temperature during the deposition of Alq₃. The thickness of Alq₃ film was monitored using a

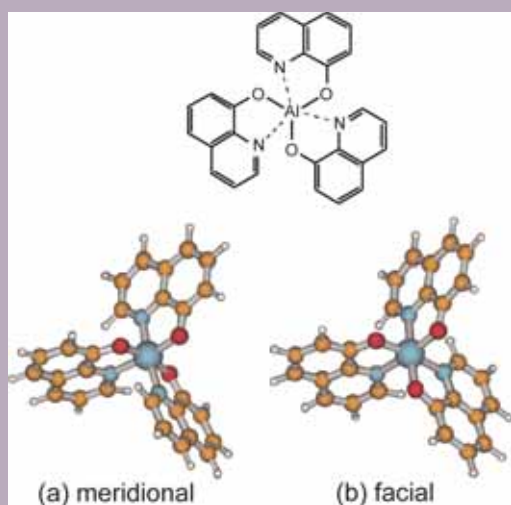


Fig. 1. The chemical structure and geometrical isomers of Alq₃.

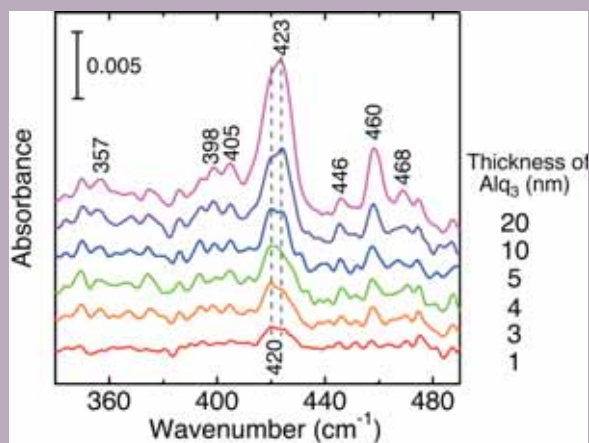


Fig. 2. The thickness dependence of the IRAS spectra of an Alq₃ film on Ag surface.

quartz microbalance. SR-IRAS spectra were accumulated with a 6 μ m-mylar beamsplitter in the Bruker system and a liquid-helium-cooled Si bolometer. Five (for 1 nm thick sample) or three (others) spectra of 100 scans each with a resolution of 2 cm⁻¹ were averaged.

Figure 2 indicates the thickness dependence of the IRAS spectra of an Alq₃ film deposited on an Ag surface. In the spectrum of the film of 1 nm thickness, corresponding to nearly one monolayer, a peak at 420 cm⁻¹ with a shoulder at 423 cm⁻¹ is observed. With increasing thickness of Alq₃, peaks at 423 and 460 cm⁻¹, which are assigned to the Al-N stretching and pyramidalization modes of the nitrogen atoms [5], respectively, increase their intensity. There are also other Al-N stretching and pyramidalization modes with different phase relation among the ligands (for example, three Al-N bonds stretch in-phase or out of phase) from those mentioned above, and they appear as weak peaks at 398 and 405 cm⁻¹ (Al-N stretching) and 446 and 468 cm⁻¹ (pyramidalization) modes, respectively [5]. Considering the central AlO₃N₃ fragment, the meridional isomer has three Al-N stretching modes with different frequencies, while the frequencies of the corresponding modes in the facial isomer are split into two, with one of them doubly degenerated because of the C₃ symmetry [5]. All of them are infrared active. The observed spectra of the Alq₃ films, except for the one with 1 nm thickness, show three Al-N stretching modes at 398, 405 and 423 cm⁻¹. This indicates that the evaporated Alq₃ film predominantly consists of the meridional isomer as reported before [2]. In the IRAS spectra of the film of 1 nm thickness, two Al-N stretching modes at 397 and 405 cm⁻¹ can not be observed. This can be understood if the molecules in the meridional form, since the estimated intensities of these peaks is only about 20% of that of the peak at 420 cm⁻¹ [5], which is the same level as the noise. In the case of the

facial isomer, on the other hand, the intensity of the peak around 398 cm⁻¹ is expected to be almost half of that of the peak at 423 cm⁻¹ [5], and this peak should be observed above the noise. In the spectrum of 1 nm thickness, however, no peak is observed at 398 cm⁻¹, and we can conclude that the meridional isomer is dominant even for the 1 nm thickness.

In the spectrum of the Alq₃ film of 1 nm thickness, the observed frequency of the Al-N stretching mode is slightly lower than that in the spectra of multilayer Alq₃. Similar “softening” of vibrational mode has been observed in the CH stretching mode of *n*-alkane adsorbed on metal surfaces, and it is ascribed to the small electron transfer from the metal to the molecule [6,7]. Moreover, DFT calculations by us show that the frequency of the Al-N stretching mode of Alq₃ anion is lower than that of Alq₃ molecule. Therefore the softening in the Alq₃/Ag system may originate from the small electron transfer from Ag to Alq₃ molecule. The observed much smaller frequency shift of the Al-N stretching mode of Alq₃ (3 cm⁻¹) than that of the CH stretching of *n*-alkanes (~100 cm⁻¹) might be understood by the larger distance between the central part of the Alq₃ and the Ag surface than that between the CH bond of flat-lying *n*-alkane molecule and the metal surface.

To summarize, thin Alq₃ films deposited on an Ag surface were investigated by IRAS using a synchrotron radiation light source. The observed IRAS spectra indicate that the Alq₃ film predominantly consists of meridional isomer including the first monolayer adsorbed on the Ag surface. In the spectrum of monolayer Alq₃, Al-N stretching mode slightly shifts to the lower wavenumber side than that of multilayer Alq₃, possibly due to the charge transfer between the Alq₃ and Ag surface.

- [1] C. W. Tang and S. A. VanSlyke, *Appl. Phys. Lett.* **51** (1987) 913.
- [2] M. Brinkmann *et al.*, *J. Am. Chem. Soc.* **122** (2000) 5147.
- [3] S. Yanagisawa and Y. Morikawa, *Chem. Phys. Lett.* **420** (2006) 523.
- [4] A. Curioni, M. Boero, and W. Andreoni, *Chem. Phys. Lett.* **294** (1998) 263.
- [5] M. Cölle *et al.*, *Phys. Chem. Chem. Phys.* **5** (2003) 2958.
- [6] M. Yamamoto *et al.*, *J. Phys. Chem. B* **104** (2000) 7363.
- [7] Y. Hosoi *et al.*, *Surf. Sci.* **515** (2002) 157.

Vacuum Ultraviolet Spectroscopy of Heavily Boron-Doped Diamonds

O. Arimoto¹, D. Gotoh², T. Katagiri³, T. Aoki³, D. Iri³, M. Itoh³

¹*Department of Physics, Kyoto Pharmaceutical University, Kyoto 607-8412, Japan*

²*Graduate School of Natural Science and Technology, Okayama University, Okayama 700-8530, Japan*

³*Department of Electrical and Electronic Engineering, Shinshu University, Nagano 380-8553, Japan*

Diamond is known as a band insulator of indirect type with a wide band gap of 5.5 eV [1,2]. By the slight doping of boron, it becomes a p-type semiconductor, making a shallow acceptor level above the top of the valence band with an activation energy of ~ 0.37 eV. With increasing boron concentration beyond the critical value $n_c \sim 2 \times 10^{20} \text{ cm}^{-3}$ for the metal-insulator (MI) transition, the boron-doped diamond shows metallic character. Recently, Ekimov and coworkers have found superconductivity in the heavily boron-doped diamond synthesized by high-pressure high-temperature (HPHT) method [3]. Subsequently, studies on the superconductivity using films made by a microwave plasma-assisted chemical vapor deposition (MPCVD) method confirmed reproducibility of the superconductivity [4]. The MPCVD method is a useful technique to control the boron density in a wide range. In order to understand the electronic structure and the mechanism of the superconductivity in heavily boron-doped diamond, various theoretical proposals and experiments such as angle-resolved photoemission spectroscopy [5] have been performed. However, systematic measurement of the fundamental optical spectra has not been done so far.

In the present study, we have performed measurements of vacuum ultraviolet reflection spectra of pure and heavily boron-doped diamonds. The top of valence band and the bottom of conduction band of pure diamond locates at the Γ point and the X point in the Brillouin zone, respectively [1,2]. The reflection spectrum is characterized by the reflection peaks at 7.4 eV and 12.6 eV. The former corresponds to the direct transition at the Γ point, while the latter to the direct transition at the X point [1,2].

All the samples used in the present study were supplied from the Kawarada's laboratory, Waseda University. Heavily boron-doped epitaxial diamond films were grown on the type Ib diamond substrates by using the MPCVD method. Figure 1 shows reflection spectra of pure and heavily boron-doped diamonds around the direct transition at the X point. Measurements were done at room temperature. The spectra (a) and (b) are for the single crystals of pure diamond (type IIa) and type Ib diamond, respectively, grown by HPHT synthesis. The spectra (c) to (e) are for the heavily doped samples. Boron concentrations of the samples B65, B67, B63 and B69 are $6.2 \times 10^{19} \text{ cm}^{-3}$, $2.8 \times 10^{20} \text{ cm}^{-3}$, $1.8 \times 10^{21} \text{ cm}^{-3}$, and $8.1 \times 10^{21} \text{ cm}^{-3}$,

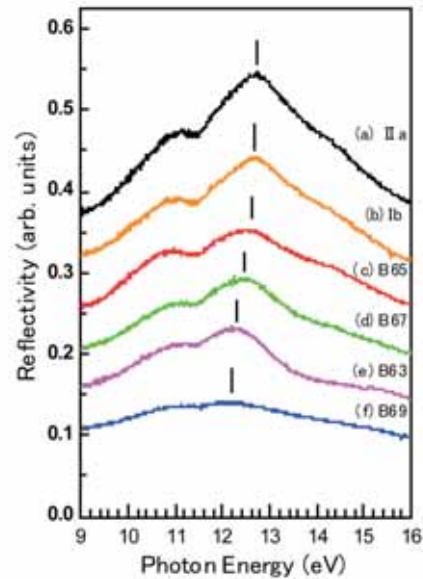


Fig. 1. Reflection spectra of pure and heavily boron-doped diamonds in the energy region of the direct transition at the X point. See text for details.

respectively. The sample B65 is insulating (semiconducting) and the sample B67 is metallic, while the samples B63 and B69 are superconducting with T_c of 2.5 K and 7.2 K, respectively. Vertical bars in the figure show the reflection peak originating from the direct transition at the X point, which locates at 12.6 eV for the pure diamond. As seen in the figure, the reflection peak shows low energy shift with increase of the boron concentration. This fact indicates that an optical energy gap at the X point becomes narrow with increase of the boron concentration. It is noteworthy that any evident energy shift was not confirmed for the reflection peak at 7.4 eV due to the direct transition at the Γ point.

- [1] W. C. Walker *et al.*, Phys. Rev. **134** (1964) A153.
- [2] W. Saslow *et al.*, Phys. Rev. Lett. **16** (1966) 354.
- [3] E. A. Ekimov *et al.*, Nature **428** (2004) 542.
- [4] Y. Takano *et al.*, Appl. Phys. Lett. **85** (2004) 2851.
- [5] T. Yokoya *et al.*, Nature **438** (2005) 647.

Photoionization of Perylene on Ionic Liquid Surfaces

N. Inoue, T. Ishioka, A. Harata

Department of Molecular and Material Sciences, Kyushu University, Kasugakoen 6-1, Kasuga-shi, Fukuoka 816-8680, Japan

Ionic liquids are rapidly expanding topics of research because of their favorable properties such as high ionic conductivity and controllable hydrophobicity. Much effort has focused on the physical properties of ionic liquids. The dielectric environment is a key factor for modeling solvent behavior because many approaches rely on dielectric continuum models for the solvent. Interfacial dielectric properties can be different from those of bulk liquids, which may distort analysis of interfacial behavior such as calculation of solvation energies of molecules across the interface. Photoionization is a suitable technique studying for interfacial process, and ionization threshold measured by this method directly reflects dielectric environment. In this report ionization threshold energies of perylene on ionic liquid were measured, and interfacial dielectric properties of ionic liquids were studied.

Ionic liquids : 1-butyl-3-methylimidazolium tetra fluoroborate, hexafluorophosphate, bistrifluoro methane sulfonylimide ([bmim][BF₄], [bmim][PF₆], and [bmim][Tf₂N]), ethylammonium nitrate ([EtA][NO₃]), and protonated betaine bistrifluoro methane sulfonylimide ([Hbet][Tf₂N]) were prepared as described elsewhere. In a typical experiment, the light was emitted from the chamber to a He-purged cell through an MgF₂ window. Light energy is in 4-8eV. The emitted light was reflected with an Al mirror and vertically irradiated on the sample surface. Applied voltage was 400V (interval length of mesh electrode and solution is 5mm). Hexane solution of perylene at 1 × 10⁻⁴M was added dropwise by 250μl onto each ionic liquid in a Pt cell of 2.5cm in diameter. After evaporation of hexane the photoinduced current (~1pA) was measured by a picoammeter (Keithly model 428).

Measured photoionization spectra were analyzed and threshold values were determined by fitting the spectra to the empirical formula of $I = (E - E_{th})^{2.5}$. Table1 shows the measured photoionization threshold of perylene on ionic liquids. In the case of [bmim][Tf₂N], current signal was below the detection limit in a vacuum. The threshold energy lies higher in a vacuum than in any other solvent because polarization energy is always exothermic and current by photoionization should have been detected within the measured range of wavelength if the perylene molecule is present at the surface of ionic liquids. It is considered that perylene molecule lies enough deep to keep photoinduced electron within [bmim][Tf₂N]. The energy required to photoionize a solute in a solu-

Table 1. Measured photoionization thresholds of perylene on ionic liquids and the relative dielectric constant of ionic liquids.

Compound	Threshold Energy / eV	Dielectric constant
[bmim][BF ₄]	6.45 ± 0.11	11.7 ± 0.6 ^[2]
[bmim][PF ₆]	6.67 ± 0.15	11.4 ± 0.6 ^[2]
[bmim][Tf ₂ N]	-	12.3 ± 0.3 ^[3]
[Hbet][Tf ₂ N]	5.12 ± 0.17	43.7 ± 0.9 ^[4]
[EtA][NO ₃]	5.97 ± 0.22	26.2 ^[5]
Water*	5.9 ± 0.1 ^[1]	80.4

*Reference

-tion satisfy $E = I_p + V_o + P_+$, where I_p stands for ionization potential of solute in vacuum, V_o conduction band energy of solvent, and P_+ polarization energy of solvent. In this experiment, V_o equals zero because electron is emitted from surface. Photoionization threshold of imidazolium based ionic liquids is lower than that in a vacuum (6.960eV). This result is consistent with that of water surface. However, P_+ is much smaller than water. It is suggested that solvation by imidazolium based ionic liquid is weak. With respect to dielectric constant, [bmim][BF₄] is larger than [bmim][PF₆], but in polarization energy, the order is in inverse. This may relate to the character that [bmim][BF₄] is more hydrophilic than [bmim][PF₆]. Some kind of attractive interaction between [bmim][BF₄] and polar species formed by photoionization or trace impurity of water may explain the results. Photoionization threshold of [EtA][NO₃] is close with that of water. It is reasonable because the dielectric constant of [EtA][NO₃] is higher than that of imidazolium based ionic liquids. Photoionization threshold of [Hbet][Tf₂N] was quite lowered. [Hbet][Tf₂N] is an ionic liquid with the ability to coordinate metal ion. This property may cause that anomalous behavior.

Dielectric environment of perylene on ionic liquids are largely influenced by the composition of ionic liquids. It is not clear that which property of ionic liquid contributes the solvation energy of perylene. Further research is in progress to clarify interfacial dielectric property of ionic liquids.

[1] Inoue *et al.*, Chem. Lett. (1998) 609.

[2] Wakai *et al.*, J. Phys. Chem. B **109** (2005) 17028.

[3] Crossing *et al.*, J. Am. Chem. Soc. **128** (2006) 13427.

[4] N.Inoue, unpublished results

[5] Weingartner *et al.*, J. Phys. Chem. A **105** (2001) 8646.

Photoluminescence in LaAlO₃ Single Crystals

K. Kanai, E. Hirata, Y. Ohki

Dept. Electrical Engineering and Bioscience, Waseda University, Shinjuku 169-8555 Japan

Lanthanum aluminate (LaAlO₃) has been attracting much attention as a promising candidate for a gate insulator in advanced metal-oxide-semiconductor devices. By analyzing photoluminescence (PL) properties of LaAlO₃, we have been examining the localized states present in the band gap that are assumed to cause leakage current.

Experimental

The samples examined are Czochralski-grown LaAlO₃ (100) single crystals, about 0.5 mm thick with both sides polished. Using synchrotron radiation under multibunch operation at the BL1B line of UVSOR Facility as a photon source, PL, PL excitation (PLE), and absorption spectra were measured at 10 K.

Results and Discussion

Figure 1 shows PL spectra of LaAlO₃ excited at 5.1 eV. Three sharp PL peaks are observed at around 1.60, 1.64, and 1.675 eV, while a broad PL peak is observed at around 2.8 eV. Figure 2 shows the PLE spectra of LaAlO₃ for each PL. Note that the PLE spectra are normalized to respective maximum intensities. The PLE spectrum detected at 2.8 eV begins to rise at around 4.5 eV, and decreases sharply at around 5.7 eV. On the other hand, the PLE spectra of the other three PLs show an abrupt rise at around 5.7 eV.

The absorption spectrum shown in Fig. 3 shows a steep rise at around 5.7 eV, namely at the energy in good agreement with the band gap energy of 5.6 eV [1]. Furthermore, the energy of 5.7 eV corresponds to the energy at which the PLE spectrum detected at 2.8 eV shows a steep decrease and to the energy at which the PLE spectra detected at 1.60, 1.64, and 1.675 eV show an abrupt increase in Fig. 2. In addition, it seems that the gradual absorption increase in the range from 4.7 to 5.7 eV corresponds to the broad peak appearing in the PLE spectrum detected at 2.8 eV. From these results, the 2.8-eV PL is assumed to be caused by electrons excited to localized states in the band gap. In contrast, the other three PLs at around 1.60, 1.64, and 1.675 eV are assumed to be caused by de-excitation of electrons excited to the conduction band.

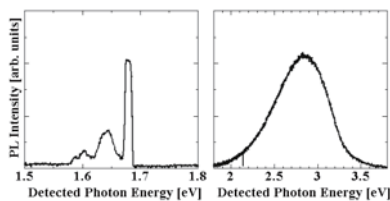


Fig. 1. PL spectra of LaAlO₃ excited at 5.1 eV.

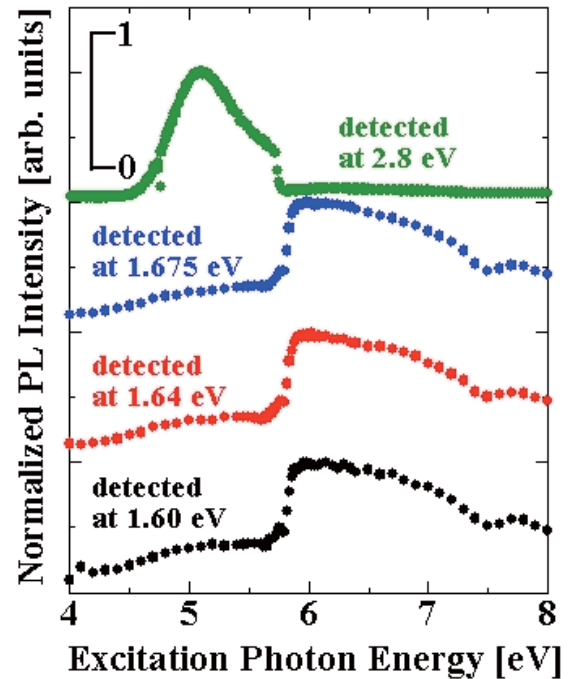


Fig. 2. PLE spectra of LaAlO₃ detected at 1.60, 1.64, 1.675, and 2.8 eV.

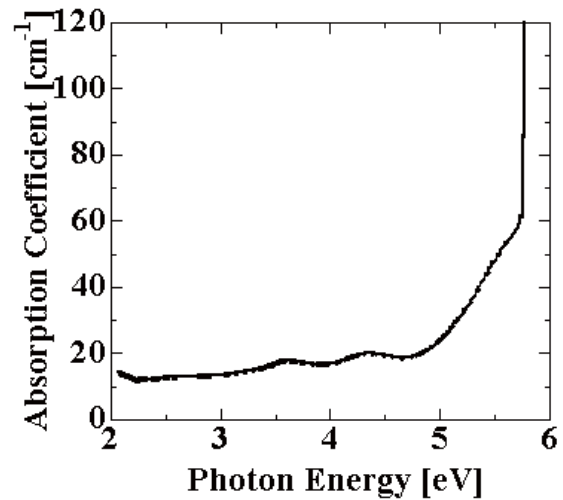


Fig. 3. Absorption spectrum of LaAlO₃.

[1] S. G. Lim *et al.*, J. Appl. Phys. **91** (2002) 4500.

Luminescence Properties of Bi₁₂GeO₂₀ (BGO) Crystals

T. Katagiri¹, D. Iri¹, T. Aoki¹, M. Itoh¹, M. Fujita², Y. Usuki³

¹Department of Electrical and Electronic Engineering, Shinshu University, Nagano 380-8553

²Japan Coast Guard Academy, Kure 737-8512

³Furukawa Co. Kannondai, Tsukuba 305-0856

Introduction

Bismuth germanium oxide, Bi₁₂GeO₂₀ (BGO), is a very efficient photoconductor and has both high sensitivity and quick response as a photorefractive crystal. However, little is known about its optical properties, as compared to another BGO (Bi₄Ge₃O₁₂) that is widely used as a scintillation material. In the present study, we have investigated reflection spectra, emission-excitation spectra, and luminescence decay kinetics of Bi₁₂GeO₂₀ crystals.

Experiment

Crystals of Bi₁₂GeO₂₀ were obtained from Furukawa Co. Reflection spectra were measured on the cleaved surfaces. Emission spectra were examined using a grating monochromator equipped with a LN/CCD camera in the temperature range $T = 5\text{--}300$ K. Luminescence decay kinetics was detected by an MCP with use of a time-correlated single-photon counting technique under the single-bunch operation of the storage ring (time duration: 1.3 ns; pulse interval: 177.6 ns).

Results and Discussion

The reflection spectra measured at $T = 5$ K showed a sharp peak at the fundamental absorption edge. This peak locating at 3.65 eV (340 nm) is naturally assigned to the excitonic transition of Bi₁₂GeO₂₀.

Figure 1 shows the emission spectra measured under the excitation with 150-nm photons at various temperatures in the range of $T = 5\text{--}45$ K. A strong band peaking at 452 nm is observed together with a very weak band around 650 nm. The intensity of the 452 nm band decreases rapidly with increasing T .

The excitation threshold of the 452 nm emission was around 3.44 eV (360 nm), which coincides with the low-energy tail region of the exciton band. This fact suggests that the 452 nm luminescence is intrinsic to Bi₁₂GeO₂₀, and arises from the radiative annihilation of the excitons that have self-trapped by inducing lattice deformation around themselves. The self-trap site could be either Bi³⁺ or O²⁻.

In Fig. 2 are shown the decay behaviors of the 452 nm luminescence measured in the range of $T = 5\text{--}45$ K. One may see two decay components: a fast one with a lifetime of nanoseconds and a slow one with a lifetime of more than 1 μ s. The latter is seen as a piled-up component. As T is increased, the lifetime of the slow component becomes shorter, resulting in reduction of the piled-up component. This result is consistent with the temperature dependence of the

emission intensity in Fig. 1.

The present work is the first observation of the intrinsic luminescence of Bi₁₂GeO₂₀.

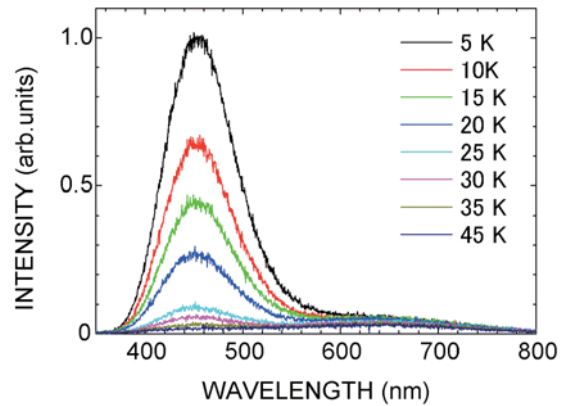


Fig. 1. Emission spectra of Bi₁₂GeO₂₀ excited at 150 nm in the temperature range $T = 5\text{--}45$ K.

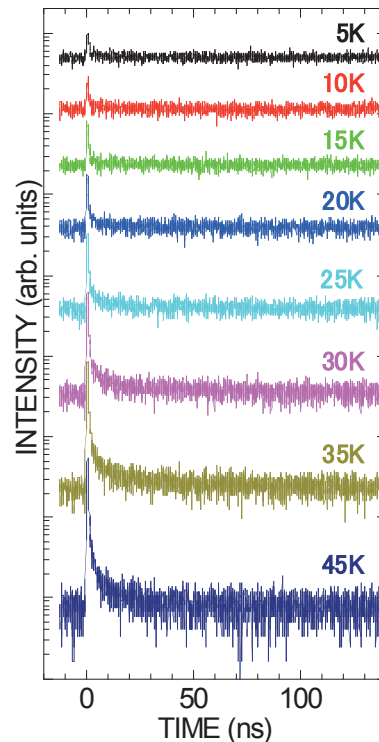


Fig. 2. Decay behaviors of the 452 nm luminescence of Bi₁₂GeO₂₀ excited at 150 nm at $T = 5\text{--}45$ K.

Optical Studies of Hydrogen-Bonded Dielectrics TiH_2PO_4

T. Kawai¹, N. Ohno²

¹Graduate School of Science, Osaka Prefecture University, Sakai 599-8531, Japan

²Graduate School of Engineering, Osaka Electro-Communication University,
Neyagawa 572-8530, Japan

Thallium dihydrogen phosphate TiH_2PO_4 (TDP) is closely related to the KH_2PO_4 (KDP) -type crystals, which are interesting hydrogen-bonded materials undergoing structural phase transitions accompanied by ferroelectricity and antiferroelectricity. In these compounds, short hydrogen bonds link PO_4 groups in three-dimensional (KDP) or two-dimensional (TDP) networks. The TDP crystal undergoes the antiferroelectric phase transition from the monoclinic $P2_1/a$ symmetry to the triclinic $C1$ symmetry at 230 K [1]. Though a number of studies on crystal structure and dielectric properties of TDP have been made above and below the phase transition temperature [1-4], optical properties and the electronic states are comparatively less studied.

In the present study, we have investigated the optical properties of TDP for the first time in UV and VUV regions at the BL-1B beam line of UVSOR. The TDP compound was synthesized by mixing stoichiometric amounts of Tl_2CO_3 and H_3PO_4 . After several times of recrystallization, crystals of TDP were grown by an ordinary evaporation method from the saturated aqueous solution.

Figure 1 shows the reflection (red curve) and absorption (blue) spectra of TDP measured at 10 K. The dip structure at 5.26 eV in the reflection spectrum is due to the reflection from the back surface of the crystal, because the energy position corresponds to that where the absorption spectrum exhibits a sharp increase. A sharp peak with dispersive structure is observed at 5.70 eV above the rise of the absorption spectrum. In the higher-energy region, several broad structures are also observed. Most of the KDP-type crystals exhibits no obvious dispersion-like structure due to the exciton transition in the reflection spectra and broad structures are observed in the energy region from 7.0 to 8.2 eV [5,6]. The broad structures of KDP have been ascribed to the transition related with the energy levels in H_2PO_4^- complex anions. The distinguished sharp

peak with dispersive structure at 5.70 eV in TDP would be the first exciton transition. It is well-known that the TI^+ impurity centers doped in the KDP-type crystals exhibit the absorption band due to the intra-cationic transition in the TI^+ ion at 5.8 eV [7,8]. Therefore, the sharp dispersion-like structure of TDP at 5.8 eV should be attributed to the exciton transition based on cationic excitation in the TI^+ ions.

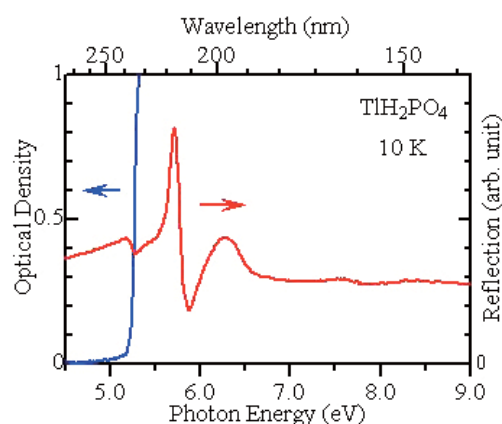


Fig. 1. Reflection spectrum (red) and absorption spectrum (blue) of TiH_2PO_4 at 10 K.

- [1] I. H. Oh *et al.*, *Acta Cryst. B* **62** (2006) 719.
- [2] N. Yasuda, S. Fujimoto, T. Asano, *Physics Lett.* **76A** (1980) 174.
- [3] H. Yoshida *et al.*, *J. Phys. Soc. Jpn.* **53** (1984) 910.
- [4] E. Alvarez-Otero *et al.*, *Acta Cryst. B* **58** (2002) 750.
- [5] S. Saito, R. Onaka, *Ferroelectrics* **21** (1978) 553.
- [6] S. Matsumoto, M. Fujisawa, S. Suga, *J. Electron. Spectrosc. Relat. Phenom.* **79** (1996) 51.
- [7] I. Fujita, *J. Phys. Soc. Jpn.* **66** (1997) 2893.
- [8] K. Ichimura *et al.*, *Phys. Status Solidi (c)* **3** (2006) 3607.

Vacuum-Ultra Violet Reflectance Spectroscopy of Orbital-Ordered Bilayer Manganites

Y. S. Lee¹, Y. Tokunaga², T. Arima³, Y. Tokura^{2,4,5}

¹*Department of Physics, Soongsil University, Seoul 156-743, Korea*

²*ERATO (Multi-Ferroids), Japan Science and Technology Agency (JST) Tsukuba 305-8562*

³*Tohoku University*

⁴*Correlated Electron Research Center (CERC) National Institute of Advance Industrial Science and Technology (AIST), Tsukuba 305-8562Japan*

⁵*Department of Applied Physics, University of Tokyo, Tokyo 113-8656 Japan*

Recent studies on strongly correlated electronic systems have revealed many unexpected phenomena due to the interplay among the spin, charge, and orbital degrees of freedom. Especially, the nanoscale self-organization and the associated complexity of electronic systems are issues of current interest. One of the representative phenomena is the concomitant charge and orbital orderings in manganites, which is involved in the metal-insulator transition with magnetic field and other various control parameters. At the lowest temperatures, the charges are ordered in a checkerboard type, forming alternating $\text{Mn}^{3+}/\text{Mn}^{4+}$ sites, and simultaneously, the e_g orbitals in Mn^{3+} sites are aligned in zigzag chain type. The direction of e_g orbital lobes defines the orbital chain and stripe. This well-organized charge, spin, or orbital ordering occurs in the *ab* plane for a variety of manganites including layered compounds.

In this beamtime, we have measured the reflectivity spectra of the bilayer manganites, $\text{Pr}(\text{Sr}_{1-x}\text{Ca}_x)_2\text{Mn}_2\text{O}_7$ (PSCMO), for $0 \leq x \leq 1$ in a photon energy range of 4 – 30 eV at room temperature using the beam line BL1B. We connected the measured spectra to the low energy ones below 5 eV, and calculated the optical conductivity spectra through the Kramers-Kronig transformation.

The bilayer PSCMO compounds exhibit an peculiar phase diagram spanning from the A-type 2D metallic phase to the charge-orbital ordered phase with the increasing x from $x = 0$. The boundary between two phases is located around $x = 0.4$. Notably, the PSCMO compounds with the ground state of the charge-orbital ordering experiences the spontaneous rotation of orbital stripe by 90° with the variation of temperature. Two successive charge-orbital ordering transitions were studied in details at a particular concentration $x = 0.9$ by performing a combination of various experimental measurements such as Dc resistivity, magnetization, optics, x-ray scattering measurements, and so on. It is noted that the ground charge-orbital ordering states turn out to be a charge polarized state due to the coincidence in the stacking patterns of the distorted bilayer Mn-O network and the charge ordering along the *c* axis.

Figure 1 shows the optical conductivity spectra for the $x = 0.2$ and 0.9 PSCMO. The dominant structures observed in optical conductivity spectra are labeled as A, B, C, and D, from the lowest energy sequence. The lowest energy of the A structure, mainly responsible for the transport, is associated with the electron hopping from Mn^{3+} to Mn^{4+} e_g bands. This structure is located at much lower energy for the $x = 0.2$ compound with the 2D metallic character than that for the $x = 0.9$ compound with the insulating charge-orbital ordering. The B structure is assigned as the charge transfer energy from O 2p to Mn e_g bands. On the other hand, it is difficult to assign structures above 5 eV as transitions with a single character, because the valence bands of four elements (Pr, Sr, Ca, and Mn) should be involved in a complicated manner. While the C structure is associated with the transitions from O 2p to Pr 3d, Ca 4s, and Sr 5s bands, the occupied Pr 5p, Ca 3p, and Sr 4p may be involved in the formation of the D structure. In this case, the strong difference in the intensity of the D structure between $x = 0.2$ and $x = 0.9$ compounds implies that the Ca 3p band should be located in much deeper than the Sr 4p band.

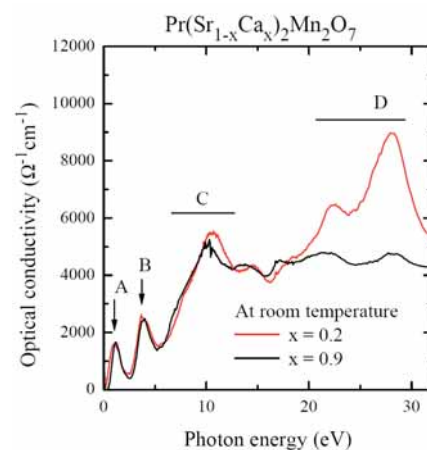


Fig. 1. Optical conductivity spectra of the $x=0.2$ (red line) and $x = 0.9$ (black line) $\text{Pr}(\text{Sr}_{1-x}\text{Ca}_x)_2\text{Mn}_2\text{O}_7$ compounds.

[1] Y. Tokura, Rep. Prog. Phys. **69** (2006) 797.

[2] Y. Tokunaga *et al.*, Nature Materials **5** (2006) 937.

Optical Properties of Sm^{2+} in KY_3F_{10}

T. Nakamura, T. Ishikawa, M. Satoh, N. Kashiwagura, M. Yamaga

Department of Mathematical and Design Engineering, Faculty of Engineering, Gifu University, Gifu 501-1193 Japan

Introduction

Rare earth ion-doped materials have been extensively studied for use in important applications such as laser, scintillator [1], and optical memory. Persistent spectral hole burning (PSHB) is applied to frequency domain optical memories. The hole burning of Sm^{2+} in disordered crystals and glasses was reported. Temperature dependence of the Sm^{2+} emission in KY_3F_{10} crystals excited by vacuum ultraviolet (VUV) and ultraviolet (UV) lights was measured, in order to examine dynamic processes of the $4f^6$ and $4f^55d^1$ excited states of Sm^{2+} in the crystal.

Experimental

Sm^{2+} doped KY_3F_{10} crystals were grown using the Bridgeman method. The optical absorption, emission and excitation spectra of Sm^{2+} in the crystal were measured using the BL1B beam line in the UVSOR. The measurement temperatures were in the range of 17-300 K.

Results and Discussion

Figure 1 shows the optical absorption, emission and excitation spectra observed in Sm^{2+} -doped KY_3F_{10} at 10 K. The absorption spectrum is composed of many bands in the wavelength range of 100-400 nm. The 160-nm excitation produces a broadband with a peak of 450 nm and three intense line groups around 560, 600, and 650 nm due to residual Sm^{3+} ions in the crystal. The 195-nm excitation produces only the 450-nm broadband. On the other hand, the emission spectrum excited at 300 nm is different from that excited at 160 nm. The emission lines around 550 and 700 nm are due to the transition from the higher energy levels of $^5\text{D}_3$ and $^5\text{D}_0$ to the lower energy levels of $^7\text{F}_J$ ($J=0-3$) of Sm^{2+} . The excitation spectra for the emission wavelengths at 500, 510, and 690 nm have the band structure in the range of 180-420 nm, being almost similar to the absorption spectrum.

Figure 2 shows the temperature dependence of the emission spectra excited at 280 nm. The 450-nm broadband and sharp lines in the range of 500-660 nm are drastically decreased above 150 K, while the sharp lines in the range 690-800 nm are almost constant up to 300 K. This result suggests that the excited states of $^5\text{D}_J$ ($J=3,2,1$) deexcite nonradiatively to the ground state with the increase of temperatures. The temperatures corresponding to the decrease of the intensities of the emission from the $^5\text{D}_J$ ($J=3,2,1,0$) excited states increase with the decrease of the number of J , that is, the emission from the the $^5\text{D}_0$ excited state is stable up to 300 K.

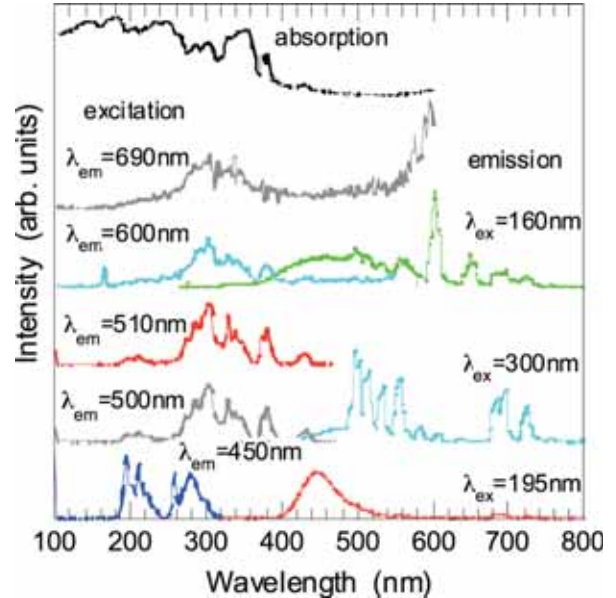


Fig. 1. Absorption, emission and excitation spectra of Sm^{2+} in KY_3F_{10} at 14 K

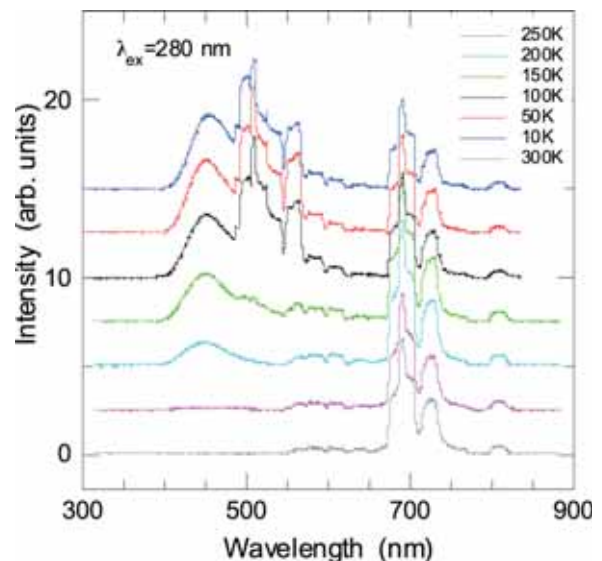


Fig. 2. Temperature dependence of the emission spectra of Sm^{2+} in KY_3F_{10} excited at 280 nm.

[1] M. Yamaga *et al.*, *J. Materials Science: Materials in Electronics* (2008) *in press*.

Luminescence Properties of $\text{YBO}_3:\text{Bi}^{3+}$ and $\text{YBO}_3:\text{Sb}^{3+}$

N. Ohno, K. Kohmoto

*Division of Electronics and Applied Physics, Graduate School of Engineering,
Osaka Electro-Communication University, Neyagawa, Osaka 572-8530, Japan*

Xe dimer (Xe_2) discharge fluorescent lamp is one of the candidates for alternative lighting sources to a conventional Hg discharge fluorescent lamp. New phosphors suitable for the conversion of vacuum ultraviolet (VUV) light into visible light are quite desired at present. In the Xe_2 discharge fluorescent lamps, phosphors are excited by VUV light of 7.2 and 8.4 eV. Most phosphate and borate hosts are transparent up to ~ 10 eV, so that the VUV light can directly excite impurity activators in these hosts. The strong absorption due to the impurity ions would give efficient conversion of the VUV light.

In the present study, luminescence properties of trivalent Ti^+ -type centers in yttrium borate have been studied in the UV and VUV region. The $\text{YBO}_3:\text{Bi}^{3+}$ and $\text{YBO}_3:\text{Sb}^{3+}$ phosphors were prepared by amounts of the appropriate starting compound powders of YBO_3 adding Bi_2O_3 or Sb_2O_3 (1 mol %), mixing and firing in a carbon crucible at 1100°C in air or nitrogen atmosphere [1]. Impurity Bi^{3+} and Sb^{3+} ions would be expected to be substituted for Y^{3+} ions in the host lattices.

Figure 1 shows luminescence (blue curve) and photo-excitation (red curve) spectra of $\text{YBO}_3:\text{Bi}^{3+}$ measured at room temperature. Luminescence peaks located at 3.8 eV and a small hump at 2.8 eV are observed for the excitation of VUV light. The 3.8 eV luminescence is excited with photons of 4.7 eV and 6–8 eV of Xe discharge energies. These excitation peaks are located at lower energies than the absorption edge of the host YBO_4 (~ 10 eV). Therefore, the observed luminescence bands of $\text{YBO}_3:\text{Bi}^{3+}$ would be responsible for intra-ionic transitions in impurity Bi^{3+} ions.

Figure 2 shows luminescence (blue curve) and photo-excitation (red curve) spectra of $\text{YBO}_3:\text{Sb}^{3+}$ at room temperature. There appear luminescence peaks at 3.6 eV and 2.9 eV for the excitation of VUV light. The 3.6 eV luminescence band is stimulated with photons of 4.7 eV and 6–8 eV. These luminescence and excitation peak energies are found to be quite similar to those of $\text{YBO}_3:\text{Bi}^{3+}$.

Ti^+ -type ions doped in alkali-halide crystals with a high symmetry crystal structure exhibit three characteristic absorption bands arising from the $s^2 \rightarrow sp$ transitions, namely, A, B and C bands [2]. These absorption bands have been attributed to the optical transition from the 1S_0 ground state to 3P_1 , 3P_2 , and 1P_1 excited states, respectively. The present study has shown that the excitation band at 4.7 eV in $\text{YBO}_3:\text{Bi}^{3+}$ and $\text{YBO}_3:\text{Sb}^{3+}$ could be tentatively

assigned as the A band nature due to $^1S_0 \rightarrow ^3P_1$ transition in Bi^{3+} and Sb^{3+} impurity ions. The excitation bands at 6–8 eV show composite structures, which is a common feature of the C band of Ti^+ -type ions. Therefore, these structures in the VUV region are ascribed to the C band originated from $^1S_0 \rightarrow ^1P_1$ transitions in Bi^{3+} and Sb^{3+} ions.

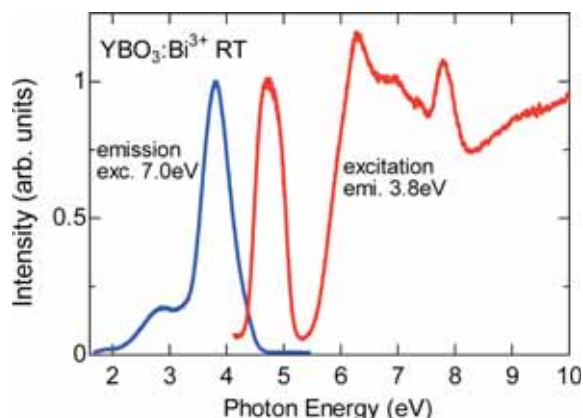


Fig. 1. Luminescence (blue curve) and excitation (red curve) spectra of $\text{YBO}_3:\text{Bi}^{3+}$ at room temperature.

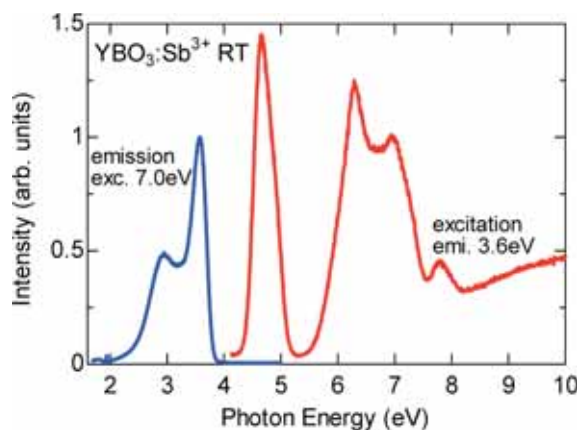


Fig. 2. Luminescence (blue curve) and excitation (red curve) spectra of $\text{YBO}_3:\text{Sb}^{3+}$ at room temperature.

- [1] X. Z. Zeng *et al.*, *J. Lumin.* **121** (2006) 1.
- [2] W. B. Fowler, *Physics of Color Centers*, Academic Press Inc., New York, 1968.

BL1B

Photoluminescence of Hydroxyapatite Irradiated by Ultraviolet Synchrotron Orbital Radiation Light (4)

M. Ohta

Department of Material Science and Technology, Faculty of Engineering, Niigata University, 8050 Ikarashi 2-no-cho, Niigata 950-2181, Japan

It was known that rare earth ions dosed for oral administration to mouse and rat are transferred to blood vessel through the ileum and deposited its teeth and bone, which mainly consists of hydroxyapatite ($\text{Ca}_{10}(\text{PO}_4)_6(\text{OH})_2$) [1-2]. Recently, rare earth is also useful as a contrast medium for magnetic resonance imaging, restriction enzyme, biocatalyst, and so on in fields of biochemistry, physiology, medicine, etc. However, the behavior of rare earth in the living body system remains an open question until now. We have found that Eu ion substituted Ba ion in Eu doped $\text{Ba}_{10}(\text{PO}_4)_6\text{Cl}_2$ phosphor, which matrix is apatite structure [3]. The Eu ions or Gd ions are also found to substitute easily for calcium ions in hydroxyapatite which is soaked in EuCl_3 or GdCl_3 aqueous solution, and to play on emission center.

In this study, hydroxyapatite samples doped with YbCl_3 aqueous solution were prepared in order to apply to phosphor. Their characteristics were investigated by photoluminescent property of Yb ion-doped hydroxyapatite samples excited by ultraviolet synchrotron orbital radiation light.

Yb-doped hydroxyapatite samples were prepared as follows: hydroxyapatite was soaked in YbCl_3 aqueous solution. After 72 hr, Yb-doped hydroxyapatite was separated from YbCl_3 aqueous solution by filtration and then dried by using with infrared ray.

The photoluminescent property of each sample excited by ultraviolet synchrotron orbital radiation light (BL-1B) was observed by using with a multi-channel analyzer.

Figure 1 shows photoluminescence spectra of Yb ion-doped hydroxyapatite samples excited by BL-1B. The photoluminescence spectra have the peak due to $^5\text{D}_{5/2} \rightarrow ^5\text{F}_{7/2}$ (about 980 nm), regardless of excitation wave length from 120 to 420 nm. The peak intensity is higher at 150 and 210 nm of excitation wave length. The peak intensity increases with the concentration of YbCl_3 aqueous solution and is held constant at from 1 to 10 mM. This fact is different from the results of Eu-doped and Gd-doped samples, reported previously [4].

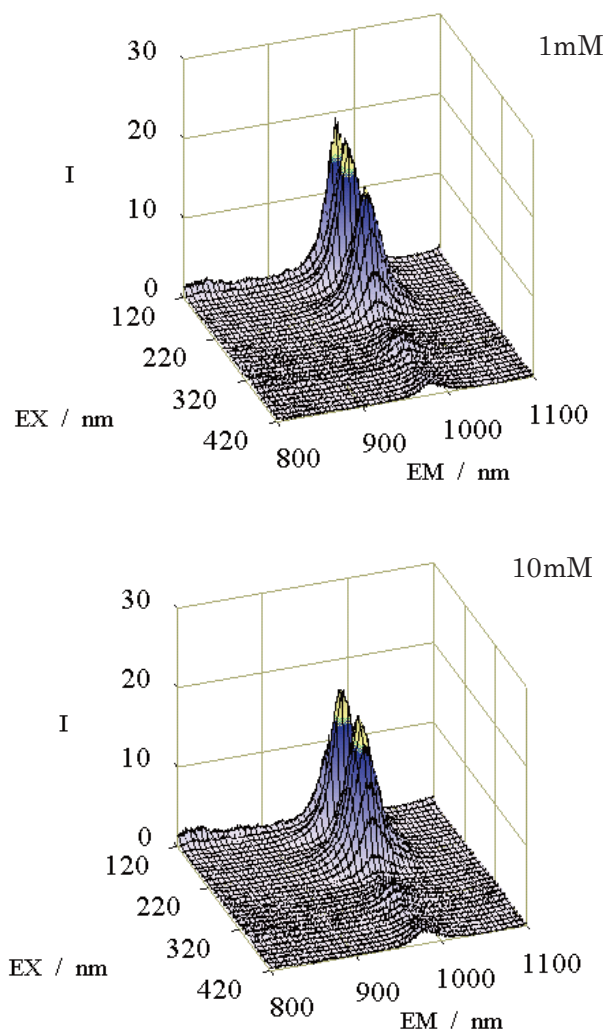


Fig. 1. Photoluminescent spectra of Yb ion-doped hydroxyapatite samples excited by ultraviolet synchrotron orbital radiation light.

[1] S. Hirano, K. T. Suzuki, *Environ. Health Perspect.* **104** (Supplement 1) (1996) 85.

[2] K. Kostial, B. Kargacin, M. Lendeka, *Int. J. Radiat. Biol. Relat. Stud. Phys. Chem. Med.* **51** (1987) 139.

[3] M. Sato, T. Tanaka, M. Ohta, *J. Electrochem. Soc.* **141** (1994) 1851.

[4] M. Ohta, *UVSOR Activity Report 2006* (2007) 75.

Effects of Curing and Filler Dispersion Methods on Dielectric Properties of Epoxy Nanocomposites

M. Okada¹, N. Hirai¹, T. Tanaka², Y. Ohki¹, T. Imai³, M. Harada⁴, M. Ochi⁴

¹ Department of EEBS, Waseda University, Shinjuku 169-8555, Japan

² Graduate School of IPS, Waseda University, Kita-Kyushu 808-0135, Japan

³ Power and Industrial Systems R&D Center, Toshiba Corp., Kawasaki 212-8582, Japan

⁴ Department of Applied Chemistry, Kansai University, Suita 564-8680, Japan

The effects of the differences in the curing and filler dispersion methods on the dielectric properties were examined for epoxy/clay nanocomposites.

The base epoxy resin is diglycidyl ether of bisphenol A cured with acid anhydride or with amine, while the clay added is montmorillonite modified by either a solubilization method or an organo method. The clay content was constant at 5 wt% throughout all the samples [1]. Table 1 shows the sample codes.

The electric conductivity was calculated by measuring the absorption current for 1000 s after the application of electric field of 10 kV/mm, while the permittivity was measured in the range of 10^{-1} - 10^7 Hz. All the above measurements were carried out at room temperature.

Using synchrotron radiation (SR) under multi-bunch operation at the BL1B line of UVSOR Facility (beam energy: 750 MeV) as a photon source, the ultraviolet (UV) photon absorbance, photoluminescence (PL) and PL excitation (PLE) spectra from the samples were measured at 10 K.

Irrespective of the filler dispersion method, both the electric conductivity and permittivity are higher in the amine-cured samples than in the acid anhydride-cured samples as shown in Figs. 1 and 2.

Furthermore, UV photon absorption becomes significantly larger at photon energies higher than 3.4 eV in the amine-cured samples and at energies higher than 4.0 eV in the acid anhydride-cured samples, irrespective of the filler dispersion method, as shown in Fig. 3. A PL band, which shows an emission peak at the energy where the UV absorption begins to increase, was found to appear in all the samples as shown in Fig. 4. From these results, the PL is due to electronic transition across the band gap, which is smaller in the amine-cured samples than in the acid anhydride-cured samples.

In most materials, the permittivity and conductivity become higher if the band gap is smaller. The present results agree with this general tendency.

Table 1. Sample codes.

	Unmodified epoxy	Solubilization Method	Organo Method
Acid anhydride curing agent	E(U)AH	C(S)AH	C(O)AH
Amine curing agent	E(U)AM	C(S)AM	C(O)AM

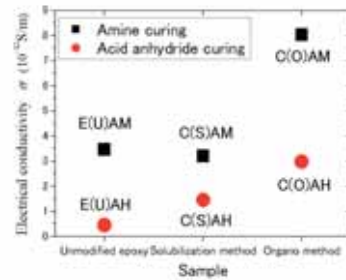


Fig. 1. Electrical conductivity (1000 [s] after voltage application).

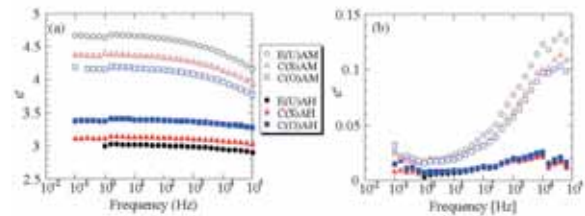


Fig. 2. Dielectric constant (a) and dielectric loss factor (b) of each sample

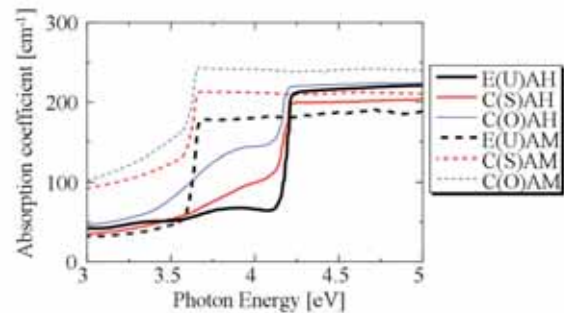


Fig. 3. Ultraviolet absorption spectra.

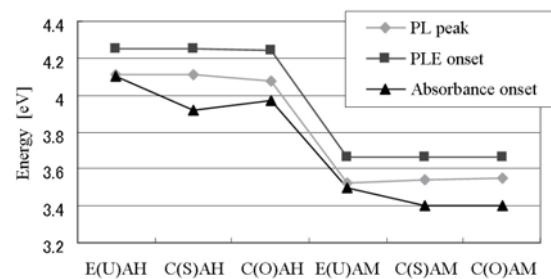


Fig. 4. PL peak, PLE onset, and absorbance onset energies.

[1] M. Harada *et al.*, Network Polymer Symposium Japan (2006) 105 (in Japanese).

The Temperature Dependence of Absorption Spectra for Heavy Lanthanides in LiYF₄ and its First-Principles Analysis

S. Watanabe¹, H. Yoshida¹, K. Ogasawara¹, M. Yoshino²

¹Department of Chemistry, Kwansei Gakuin University, 2-1 Gakuen, Sanda 669-1337 Japan

²Department of Materials, Physics and Engineering, Nagoya University, Furo-cho, Chikusa-ku, Nagoya, 464-8603, Japan

The divalent or trivalent lanthanide ions in wide band gap host crystals or glasses have drawn attentions due to their application for luminescent materials in UV and VUV regions such as solid-state lasers or phosphors. In those materials, the trivalent lanthanide ions (Ln³⁺) in LiYF₄ crystal have been well known as exquisite luminescence centers.

In this work, we have investigated the temperature dependence of $4f^n-4f^{n-1}5d^1$ absorption spectra for heavy lanthanides in LiYF₄ host crystal. As the luminescence centers, we adopted the three heavy lanthanide ions, which are Terbium (Tb³⁺), Dysprosium (Dy³⁺) and Erbium (Er³⁺). And we also analyzed the spectra based on the first-principles calculation for multiplet energy and absorption spectrum using the 4-component relativistic configuration interaction (CI) method [1]. This calculation method has been successfully applied to calculation of the multiplet energy levels and optical absorption spectrum between multiples for impurity ions in host crystals [2]. By measurements of the absorption spectrum at low temperature, we could directly compare the theoretical absorption spectrum to that obtained by the first-principles calculation. Therefore, the combination of measurements of the absorption spectrum at low temperature and first-principles calculations is very effective procedure for analysis of optical properties.

The LiYF₄ single crystal doped with Ln³⁺ (Ln³⁺=Tb³⁺, Dy³⁺, Er³⁺) were grown by Bridgman-Stockbarger method. The concentration of Ln³⁺ in the sample was 0.3 mol%.

Fig. 1 shows the temperature dependence of experimental absorption spectra and the theoretical absorption spectrum for Dy³⁺ in LiYF₄.

The $4f^9-4f^85d^1$ absorption spectrum for Dy³⁺ in LiYF₄ is observed by using the SR source for the first time. The experimental absorption spectra were very complicated and did not strongly depend on temperature except for the peak D, E. These results indicate that the configuration interaction of each multiplet is very strong. In addition to Dy³⁺ impurity absorption, the absorption of LiYF₄ host crystal was observed above about 10.8 eV.

The theoretical spectrum is in good agreement with experimental one. Though the absolute multiplet energy levels are not reproduced exactly, the relative peak position and shapes of absorption spectrum are

reproduced fairly well without any empirical parameters.

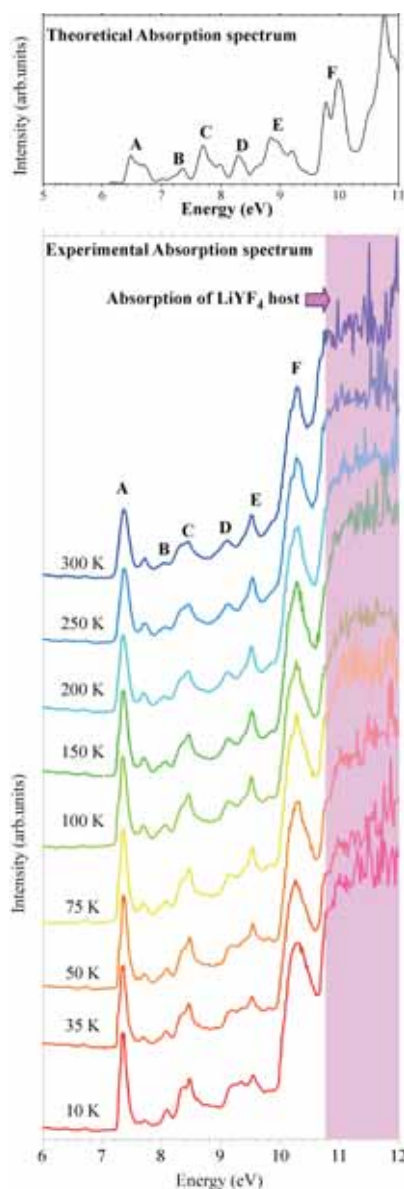


Fig. 1. The theoretical absorption spectrum and the temperature dependence of experimental absorption spectra for Dy³⁺ in LiYF₄.

[1] K. Ogasawara *et al.*, Phys. Rev. B **64** (2001) 143.

[2] K. Ogasawara *et al.*, J. Solid State Chem. **178** (2005) 412.

Excitation Spectra for Lanthanides in YAG and its First-Principles Analysis

M. Yoshino¹, S. Watanabe², H. Yoshida², K. Ogasawara²

¹*Department of Materials, Physics and Energy Engineering, Nagoya University, Nagoya
464-8603, Japan*

²*Department of Chemistry, Kwansei Gakuin University, Sanda 669-1337, Japan*

The trivalent lanthanide ions (e.g. Nd^{3+} , Er^{3+} , Yb^{3+}) in $\text{Y}_3\text{Al}_5\text{O}_{12}$ (YAG) crystals have drawn attentions due to their application for luminescent materials in NIR to UV regions such as solid-state lasers or phosphors. And, Pr^{3+} and Tb^{3+} have also attracted attentions as luminescence centers. In this work, the $4f^n-4f^{n-1}5d^1$ excitation spectra and emission spectra for lanthanides in YAG crystal have been measured. As the luminescence centers, Pr^{3+} and Tb^{3+} are used. The lanthanides ion doped YAG samples are produced by solid state reactions. The concentration of Ln^{3+} in the samples are 3 mol%. And the spectra are analyzed based on the first-principles calculation for multiplet energy and absorption spectrum using the relativistic configuration interaction (CI) method [1]. This calculation method has been successfully applied to calculation of the multiplet energy levels and optical absorption spectrum for impurity ions in hosts [2]. Fig. 1 shows the experimental excitation spectrum for Pr^{3+} in YAG. The two peaks exist around 4-6 eV correspond to the $4f^2-4f^15d^1$ absorption. And the spectrum above about 6.5 eV relates to absorption of YAG host. And this sample shows strong emission in VIS region as shown in Fig. 2. Fig. 3 shows the theoretical absorption spectrum for Pr^{3+} in YAG. Though the absolute multiplet energy levels are not reproduced, the shapes and distribution of peak position in excitation spectrum are roughly reproduced without any empirical parameters. The experiments and calculation are also examined about Tb^{3+} in YAG (Fig. 4).

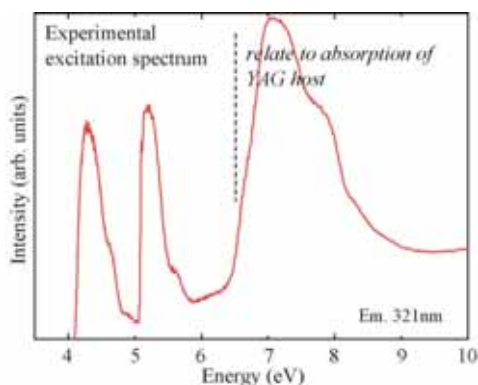


Fig. 1. Experimental excitation spectrum for Pr^{3+} in YAG.

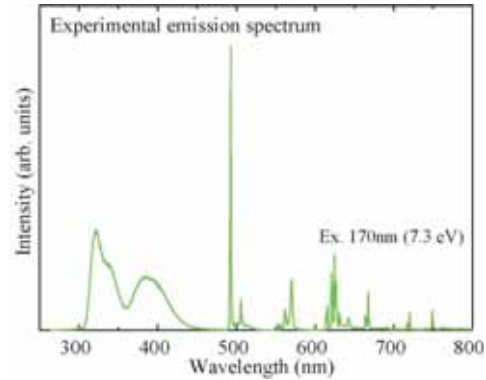


Fig. 2. Experimental emission spectrum for Pr^{3+} in YAG.

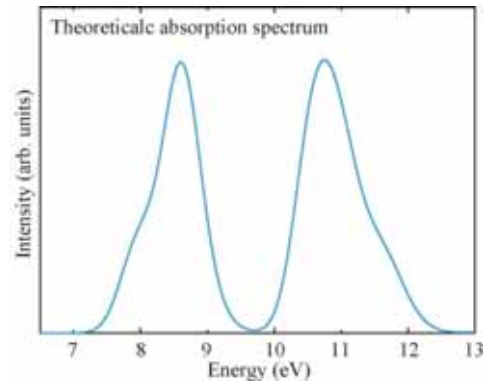


Fig. 3. Theoretical absorption spectrum for Pr^{3+} in YAG.

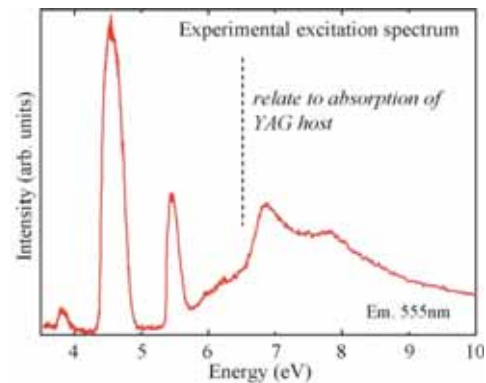


Fig. 4. Experimental excitation spectrum for Tb^{3+} in YAG.

[1] K. Ogasawara *et al.*, Phys. Rev. B **64** (2001) 143.

[2] K. Ogasawara *et al.*, J. Solid State Chem. **178** (2005) 412.

BL5B
Absorption Spectra of Dilute Magnetic Semiconductor GaCrN in VUV Region

S. Emura, S. Kimura, Y. Hiromura, H. Asahi
ISIR, Osaka University, Mihoga-oka 8-1, Ibaraki, Osaka 567-0047

In present society, infrastructures of communication are demanded to expand in the speed and the quantity. One of future devices in this field is a spin-related device. Several candidates are considered and a part of those starts in fundamental research. Theoretical study also reveals the possibility of dilute magnetic semiconductor that exhibits ferromagnetism at room temperature and predicted that GaN-based dilute magnetic semiconductors, especially Cr-doped GaN, are highly potential candidates for those materials. This material, Cr doped wide gap semiconductor, shows ferromagnetic properties even at 400K experimentally. This is one of highest Curie temperatures at present in dilute magnetic semiconductors. Furthermore, GaCrN substance emits luminescence at the energy of near the band gap of Ga. We have, thus, three independent characters for GaCrN, semiconductor nature, ferromagnetism, and optical feature.

The origin of the magnetic behaviors of dilute magnetic semiconductors based on nitride is still open in discussion, though several first-principles calculations, as described above, appeal to the public. It seems that their predictions do not clearly explain magnetic characteristics such as the dependence of the magnetic strength on the magnetic dopant concentration, peculiar form of M – H curve, and the weak hysteresis.

The growth of cubic-GaN:Cr layers was performed on MgO (001) substrates by radio frequency (RF) plasma-assisted molecular beam epitaxy techniques. Sources used here were elemental Ga and Cr and plasma-excited nitrogen. After thermally cleaning of MgO substrate surfaces, several monolayer of GaN were grown at low substrate temperature (540°C) and then 50 nm of cubic-GaN buffer layer was grown at 700°C. On the cubic-GaN buffer layer, cubic-GaCrN layer with approximately 100 - 200 nm in the thickness was grown as a function of Cr cell temperature ($T_{Cr} = 810 - 1030^\circ\text{C}$). The fixed nitrogen flow rate (1.5 SCCM) with the fixed plasma power (180 W) was supplied during growth for all of the cubic-GaN:Cr layers. Growth rate and slightly N-rich condition of V-III ratio were kept constant for all the samples grown at different substrate temperatures. Therefore, the Ga flux of 1.9, 1.6 and 1.3×10^{-7} Torr was used for the substrate temperature of 700, 540 and 350°C respectively because evaporation of Ga atoms is suppressed on the grown surface at lower temperature. Finally, GaN layer with 10 nm in the thickness was deposited to avoid the oxidation of

GaN:Cr layer surfaces.

In consideration of the electronic state of Cr in GaN matrix to survey the origin of the ferromagnetism of GaCrN, the molecular orbital schema of CrN_4 is important. The molecular orbitals of $(\text{CrN}_4)^{-9}$ are resolved in tetrahedral symmetry by group theory as follows,

$$\text{N-}2p: a_1 + e + t_1 + 2t_2 \text{ (} a_1 \text{ and } t_2 \text{ are } \sigma \text{ orbitals)} \quad (1)$$

$$\text{N-}2s: a_1 + t_2 \quad (2)$$

$$\text{Cr-}3d: e + t_2 \quad (3)$$

The schematic semi-quantitative diagram is shown in Fig.1. The quantitative parts in the figure are deduced from the combination of 1s core absorption spectra and VUV absorption spectra observed. The three electrons belonging to the magnetic dopant Cr atom occupy with a manner of two kinds, so-called, low spin state and high spin state. The present problem is which state is preferable. It strongly affects the ferromagnetism of this system GaCrN. The VUV dichronic and ESR measurements are necessary to confirm whether the Cr state takes low or high spin state.

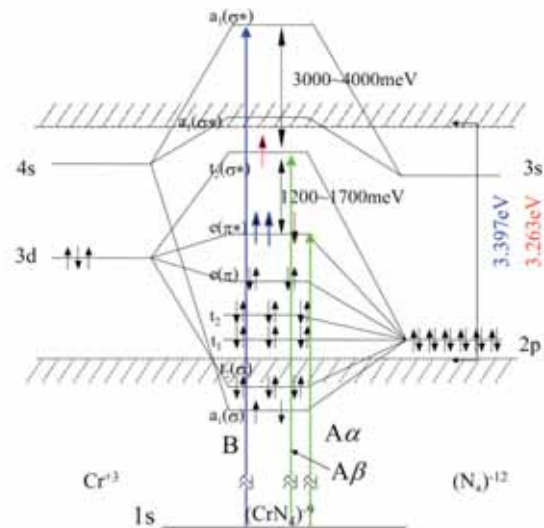


Fig. 1. Schematic energy diagram of the $(\text{CrN}_4)^{-9}$ molecular.

Photostructural Changes in Amorphous Chalcogenide Materials

K. Hayashi

Department of Electrical and Electronic Engineering, Gifu University, Gifu 501-1193, Japan

Introduction

It is well-known that amorphous chalcogenide materials exhibit a variety of photoinduced phenomena by irradiation of light with energy corresponding to the optical band gap [1]. Photoinduced changes observed in amorphous chalcogenide materials are classified into two types, irreversible and reversible changes. Reversible changes can be induced optically in amorphous bulk materials and well-annealed evaporated thin films, in which the changes can be removed by annealing to the glass-transition temperature. The reversible photodarkening arising from the red-shift of the optical absorption edge is a typical reversible photoinduced phenomenon. Irreversible changes are induced in as-deposited evaporated thin films. The irreversible photodarkening in as-deposited amorphous films is an irreversible change, it is believed that it occurred by photo-polymerization. The irreversible changes observed in EXAFS [2-3] and IR [4] are interpreted by rearrangement of bonding configurations of molecular species within as-deposited evaporated films.

To our knowledge, little attention has been given to photoinduced changes at the vacuum ultra-violet (VUV) absorption spectrum. In this report, we investigate photoinduced changes at the VUV transmission spectra on as-deposited evaporated films and well-annealed evaporated films.

Experimental

Thin films of amorphous chalcogenide semiconductor ($a\text{-As}_2\text{S}_3$ and $a\text{-As}_2\text{Se}_3$) were prepared onto ultrathin collodion films by conventional evaporation technique. A typical thickness of an amorphous film was around 200nm. The ultrathin collodion films were prepared onto stainless steel metal plates in which two pinholes of the 1.0mm diameter opened. A xenon arc lamp with IR-cut-off filter was used as a light source. Before the measurement of the VUV transmission spectrum, the unilateral of the sample was irradiated with the light in a vacuum to the degree in which the sample sufficiently produced the photodarkening. The measurement of the VUV transmission spectra were carried out at room temperature at the BL5B beam line of the UVSOR facility of the Institute for Molecular Science. And the spectrum was measured by using the silicon photodiode as a detector. To eliminate the higher order light from the monochromator, an aluminum thin film was inserted between the monochromator and sample. We also monitored the spectrum of the light source by measuring the total photoyield of a gold mesh.

Results and Discussion

Figure 1 shows the VUV transmission spectrum of an as-deposited $a\text{-As}_2\text{Se}_3$ film at room temperature in the photon energy region between 40 and 65eV. Two main absorption peaks were observed in this energy region. One absorption peak around 44eV corresponds to the 3d core level of As atom. Another absorption peak around 57eV corresponds to the 3d core level of Se atom. As shown in the Fig. 1, the spectral line width of that absorption is very broad and multiple shoulders are observed. A similar spectrum is observed in the as-deposited $a\text{-As}_2\text{S}_3$ film. It can be attributed to the spin-orbit splitting of the 3d core level of each atom as observed by XPS. As for the origins of the shoulders, it is not clear. I think that these shoulders are related to the local structures of the amorphous network. The detailed experiments and analysis will be done in the next step.

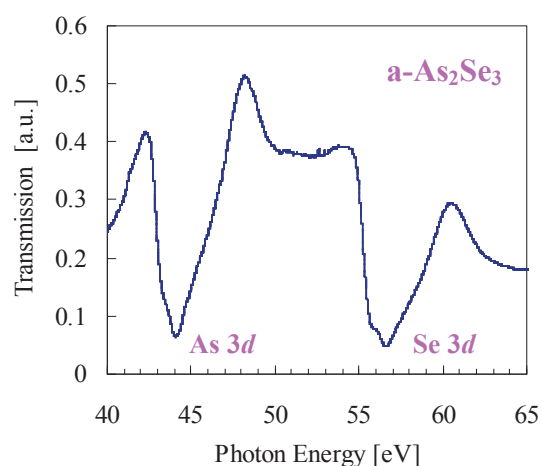


Fig. 1. The VUV transmission spectrum of an as-deposited $a\text{-As}_2\text{Se}_3$ film.

Acknowledgements

This work was partly supported by Research Foundation for the Electrotechnology of Chubu.

- [1] Ke. Tanaka, *Rev. Solid State Sci.* **4** (1990) 641.
- [2] J.P. De Neuvile, S.C. Moss, and S.R. Ovsinsky, *J. Non-Cryst. Solids*, **13** (1973/1974) 191.
- [3] A.J. Lowe, S.R. Elliot, and G.N. Greaves, *Philos. Mag. B* **54** (1986) 483.
- [4] S. Onari, K. Asai, and T.Arai, *J. Non-Cryst. Solids* **77&78** (1985) 1215.

Optical Oscillator Strength Distribution of Amino Acids from 3 to 250 eV and Examination of the Thomas-Reiche-Kuhn Sum Rule^[1]

M. Kamohara, Y. Izumi, M. Tanaka, K. Okamoto, K. Nakagawa*
*Graduate school of Human Development and Environment, Kobe University,
 Tsurukabuto, Nada-ku, Kobe 657-8501, Japan*

Absorption spectra of amino acid films were measured in the photon energy range of vacuum ultraviolet (VUV) and soft X-ray region in an attempt to examine the validity of the Thomas-Reiche-Kuhn oscillator strength sum rule.

Thin films of glycine (Gly), alanine (Ala), phenylalanine (Phe), and methionine (Met) were prepared by the vacuum sublimation technique on the collodion substrates.

Absorption spectra were measured at the beamline 5B and 7B of the synchrotron radiation facility UVSOR in the Institute of Molecular Science, Okazaki, Japan. Values of optical absorption cross section $\sigma(E)$ at photon energy E were translated into the optical oscillator strength distribution df/dE . An example of obtained results for Met films is shown in Fig. 1, in which large peak from 10 eV to 70 eV is due to transitions between valence levels and small peak from 170 eV to 250 eV was due to transitions from 2s and 2p levels of sulfur atom of Met.

According to the Thomas-Reiche-Kuhn oscillator strength sum rule, integrated value f_{total} of df/dE should be equal to the number of electrons N_e associated to the optical transition within the energy range of integration. After careful examinations, we obtained values of f_{total} and N_e to be 27.3 and 30 for Gly, 31.0 and 36 for Ala, 63.2 and 64 for Phe, and 60.1 and 62 for Met, respectively. We concluded that the T-R-K sum rule meets in a good manner for amino acid molecules.

This work was done through the joint programs of the Institute for Molecular Science, 18-515 and 18-534.

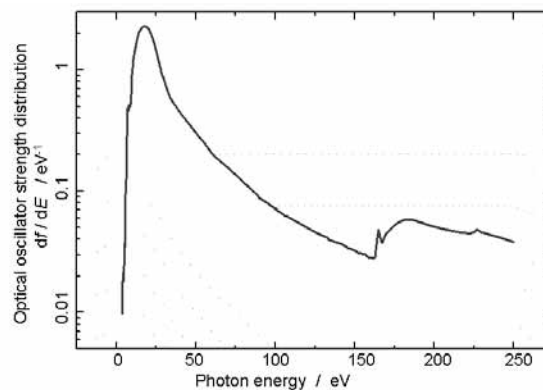


Fig. 1. Optical oscillator strength distribution of methionine thin film.

*Corresponding author: nakagawa@kobe-u.ac.jp

[1] M. Kamohara *et al.*, *J. Rad. Phys Chem.* (2008) *in press*.

Far-Infrared and Millimeter Wave Spectroscopy of Superionic Copper Conductors

T. Awano

Department of Electronic Engineering, Tohoku Gakuin University, Tagajo 985-8537, Japan

Superionic conductors have high ionic conductivity as liquid or electrolyte solution. Far-infrared and millimeter wave region corresponds to the frequency boundary between translation and vibration movement of conduction ion. Spectroscopic study of this frequency region, therefore, seems to make characteristic dynamics of mobile ions in superionic conductors, such as correlative collective movement of mobile ions clear.

$\text{RbCu}_4\text{Cl}_{3+x}\text{I}_{2-x}$ crystals have the highest ionic conductivity at room temperature and have the same structure as RbAg_4I_5 . Therefore this is a suitable system to compare dynamics of mobile ions.

Fig. 1 shows absorption spectra of $\text{RbCu}_4\text{Cl}_{3.25}\text{I}_{1.75}$ crystal obtained by K-K analysis from reflectivity spectra. Broad absorption peak was observed around 40, 80 and 110-200 cm^{-1} at room temperature. These bands have doublet structure at low temperature. This seems to be due to difference of local structure by chlorine and iodine ion. The number of couples of cations and chlorine or iodine ions is comparable and absorption intensity seems to be almost equal.

The 110-200 cm^{-1} bands seems to be symmetric breathing modes of CuX_4 ($X = \text{Cl}$ or I) tetrahedron. In CuI , TO phonon frequency is 130 cm^{-1} and 170 cm^{-1} in CuCl . These bands were observed around 100-120 cm^{-1} in RbAg_4I_5 . This frequency shift coincides with the inverse of square root of the mass ratio of conduction ions.

The 80 cm^{-1} band seems to be Rb-X vibration in RbX_6 octahedron. In RbI , the frequency of TO phonon is 80 cm^{-1} .

The 40 cm^{-1} band seems to be the attempt mode which is an outward motion of the mobile ion in halogen cage. In silver conductors, the attempt mode is observed around 20 cm^{-1} [1]. This frequency shift coincides with the inverse of square root of the mass ratio of conduction ions.

Reflectivity at low energy side increased at room temperature. This is due to translational movement of conduction ion. Correlation of ionic movement by coulomb repulsion seems to occur because the number of available site for conduction ion is not so many and the distance between them is not so large. Such a collective movement in phase is able to be regarded as "ionic plasmon". Plasmon fitting by Drude model in energy loss function spectra of $\text{RbCu}_4\text{Cl}_{3.125}\text{I}_{1.875}$ is shown in fig. 2. Energy loss function, $\text{Im}(1/\epsilon)$, is proportional to absorption intensity by transverse wave. The dotted line shows calculated one from the Drude model. The fitting curve well coincides with the energy loss function spectrum of the spectral region below the attempt

mode, i.e. below 35 cm^{-1} , at 298 K. The plasmon frequency, 45 cm^{-1} , in the fitting parameters is proportional to the inverse of square root of mass ratio of silver and copper ion, comparing with those in MAg_4I_5 [1] i.e. 26-27 cm^{-1} . The plasmon fitting was impossible for the spectra at low temperatures. This means that such a movement in phase needs kinetic energy of the conduction ion much larger than the activation energy of the ionic conduction.

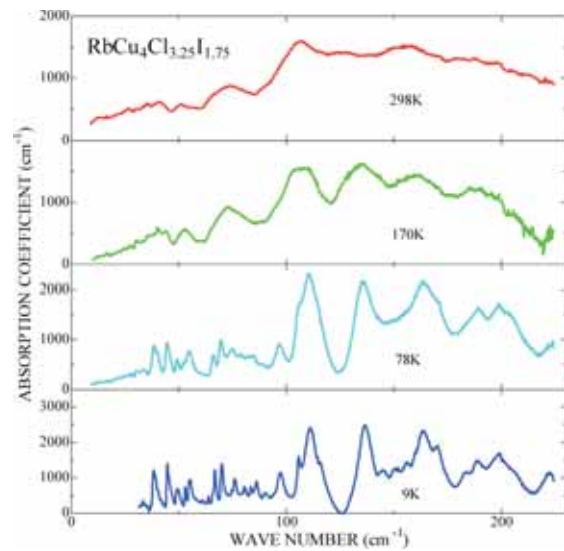


Fig. 1. Absorption spectra of $\text{RbCu}_4\text{Cl}_{3.25}\text{I}_{1.75}$.

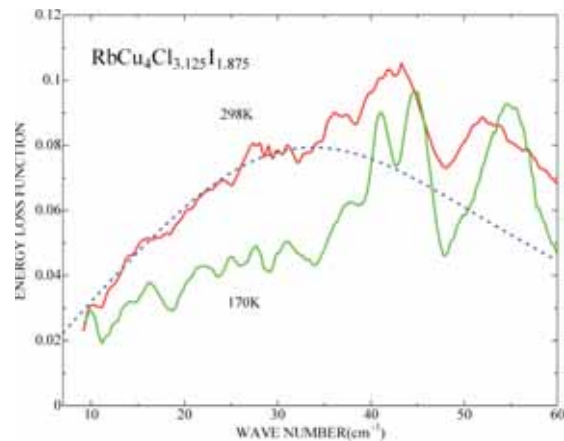


Fig. 2. Energy loss function spectra of $\text{RbCu}_4\text{Cl}_{3.125}\text{I}_{1.875}$.

[1] T. Awano, T. Nanba, M. Ikezawa, Solid State Ionics **53-56** (1992) 1269.

Infrared Spectroscopy on CeIn₃ under Pressure

T. Iizuka¹, T. Mizuno¹, K. E. Lee², H. J. Im^{2,3}, Y. S. Kwon², S. Kimura^{3,1}

¹*School of Physical Sciences, The Graduate University for Advanced Studies (SOKENDAI), Okazaki 444-8585, Japan*

²*Department of Physics, Sungkyunkwan University, Suwon 440-746, Korea*

³*UVSOR Facility, Institute for Molecular Science, Okazaki 444-8585, Japan*

Introduction

In recent years, some compounds called “heavy fermion” (HF) attract attention because of their various physical properties. The physical properties originate from the hybridization between itinerant conduction electrons and local $4f$ electrons. One of the characteristic physical properties is superconductivity due to the HF, which appears near a quantum critical point (QCP) located in between the local and itinerant characters of $4f$ electrons. There are many experimental and theoretical studies to clarify the origin of the various physical properties at QCP. The various physical properties originate from electronic structure near the Fermi level. To investigate the electronic state at QCP and the translation process from local to itinerant character of $4f$ electrons, we measured reflectivity spectra of CeIn₃ that is an AuCu₃-type cubic intermetallic HF compound with a magnetic ground state resulting from the competition between long ranged antiferromagnetism ($T_N=11\text{K}$), which is produced by RKKY interaction, and the Kondo effect. With applying pressure, the ground state changes from antiferromagnetic to nonmagnetic HF state via the QCP [1]. Therefore this material is suitable to investigate the electronic structure around the QCP.

Experimental

The single crystalline CeIn₃ sample was synthesized by an arc melting under argon atmosphere, and then annealed at 600 °C for three weeks inside an evacuated quartz tube. The THz reflection spectroscopy under pressure was performed at the THz micro-spectroscopy end station of UVSOR-II BL6B. A diamond anvil cell was employed to produce high pressure. KBr was used as a pressure medium and a gold film as a reference. The pressure was calibrated by a ruby fluorescence method.

Results and Discussion

We obtained pressure-dependent reflectivity spectra [$R(\omega, P)$] of CeIn₃ at 300K in the pressure region from 0.7 to 5.6 GPa as shown in Fig. 1. The spectra were divided by that at 0.7 GPa to emphasize the pressure dependence. With increasing pressure, the $R(\omega, P)$ intensity around 0.75 eV was enhanced.

To explain the pressure-dependent of $R(\omega, P)$, an interpretation using the periodic Anderson model (PAM) has been employed by Hancock *et al.* [2] and

Okamura *et al.* [3], previously. In their interpretation, the reflectivity peak in the middle infrared region originates from the optical transition in between the bonding and antibonding states of the hybridization band of the conduction and local $4f$ electrons predicted with PAM. Due to the PAM, the $R(\omega, P)$ peak must shift to the higher energy side. However, in this study, the $R(\omega, P)$ peak does not shift with increasing pressure. The result is not consistent with the prediction of PAM. This result suggests that the interpretation by usual PAM is insufficient. Recent theoretical study on YbAl₃ indicates that the infrared peak originates from the band structure including the hybridization between the conduction and $4f$ electrons [4]. Our result is consistent with the theoretical work.

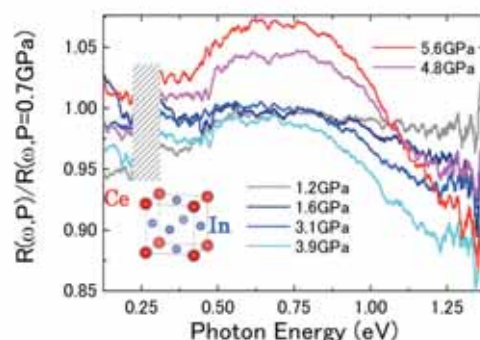


Fig. 1. Reflectivity spectra [$R(\omega, P)$] of CeIn₃ with AuCu₃-type cubic crystal structure (inset) under pressure at 300K divided by that at 0.7 GPa. The hatched area is that $R(\omega, P)$ cannot be measured because of an absorption of the diamond.

[1] S. Kawasaki *et al.*, J. Phys. Soc. Jpn. **73** (2004) 1647.

[2] J. N. Hancock *et al.*, Phys. Rev. Lett. **92** (2004) 186405.

[3] H. Okamura *et al.*, J. Phys. Soc. Jpn. **76** (2007) 023703.

[4] H. Kuroiwa *et al.*, J. Phys. Soc. Jpn. **76** (2007) 124704.

Phonon-Polariton of Superconducting InN Observed by Far-Infrared Synchrotron Radiation

T. Inushima¹, Y. Ota¹, T. Yanagawa², K. Fukui²

¹Department of Electronics, Tokai University, Hiratsuka, 259-1292 Japan

²Department of Electronics and Electrical Engineering, University of Fukui, Fukui 910-8507 Japan

Temperature dependence of the reflectivity of superconducting InN with a carrier concentration of $3.5\sim 4.7\times 10^{17}\text{cm}^{-3}$ is investigated from 50 to 750 cm^{-1} using infrared synchrotron radiation. E_1 phonon is observed separately from plasma oscillation, and in the energy range below $E_1(\text{TO})$, phonon-polariton is observed up to 10^4cm^{-1} . The lifetime of the $E_1(\text{TO})$ phonon is directly determined by the reflectivity measurements. From the temperature dependence of the lifetime, it is concluded that the $E_1(\text{TO})$ phonon decays primarily into phonons with a renormalized frequency of 177cm^{-1} . From the plasma edge position the electron effective mass is estimated to be $m_e=0.076m_0$ for the intrinsic InN.

All of the InN films investigated had a hexagonal structure and their c-axes were perpendicular to the sapphire (0001) planes. Therefore, one E_1 optical phonon was observed in this configuration. Figure 1 shows the reflectivity spectrum of GS1586 ($n_e=3.5\times 10^{17}\text{cm}^{-3}$). In the spectrum there is a clear Reststrahlen band around 500cm^{-1} , which is due to the E_1 optical phonon. A reflection edge due to the plasma oscillation is observed at 200cm^{-1} . The reflectivity spectrum is analysed using a following dielectric function,

$$\varepsilon(\omega) = \varepsilon_0 + \frac{\omega_p^2}{\omega^2 - i\omega\gamma} + \frac{\omega_{\text{TO}}^2 - \omega^2}{\omega^2 - \omega_{\text{TO}}^2 + i\omega\Gamma}. \quad (1)$$

Using Eq. 1, the reflectivity spectrum is well reproduced and fitting parameters are obtained.

As is seen in Fig.1, the oscillations below $E_1(\text{TO})$ are due to the interference of the penetrating light in the InN film. In this case, the light with momentum k is expressed by polariton and is expressed using $\varepsilon(\omega)$ of InN as follows,

$$\frac{c^2 k(\omega)^2}{\omega^2} = \varepsilon(\omega); \quad k(\omega) = \frac{N\omega\lambda}{2cd}. \quad (2)$$

The observed phonon-polariton dispersion is shown in Fig. 2. In this experiment, the phonon-polariton is observed up to 1.2eV (10^4cm^{-1}).

The ratio of $\Gamma/\omega_{\text{TO}}$ is the energy dissipation rate for the E_1 vibration. When we regard this as an unharmonic factor of the crystal, InN has 3.3×10^{-3} , which is comparable to those of III-V compounds, indicating that the crystal growth technology of InN has attained the level of major III-V compounds. Nevertheless, the InN investigated here shows superconductivity. Once it was proposed that the

In-In nano-structure spread in the a - b plane was the cause of the occurrence of the superconductivity[1]. The results presented here show that there is no such structure in InN. At present we have to conclude that InN has strong electron-phonon and electron-electron interactions and the superconductivity is induced by this effect.

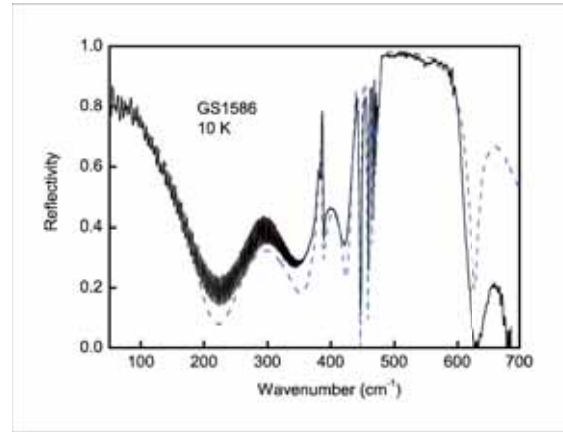


Fig. 1. Reflection spectrum of GS1586 at 10 K. The fitted line (blue line) is drawn using Eq. 1. The fitting parameters are; $\omega_p=0.03\text{eV}$, $\omega_{\text{TO}}=0.0594\text{eV}$, $\varepsilon_0=10.3$, $\Gamma=0.0002\text{eV}$, $\gamma=0.008\text{eV}$, $\varepsilon_\infty=6.7$, $d=4.2\text{um}$.

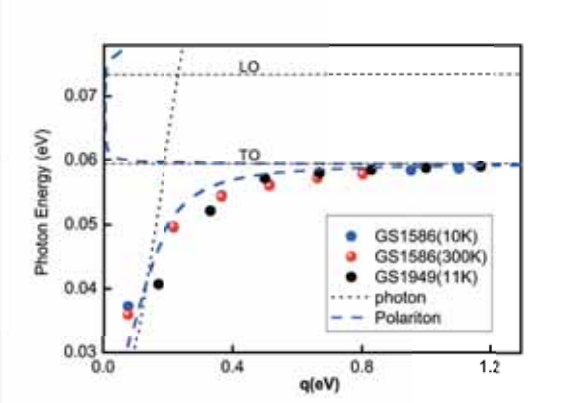


Fig. 2. Phonon-polariton wavenumber $q=\hbar k$ is plotted against photon energy $\hbar\omega$. The data points are obtained at the peak positions shown in Fig. 1, where the order starts at the peak at 300cm^{-1} , where $N=0.5$. The dashed line is drawn using $\varepsilon(\omega)$ given in Eq. 2, and the dotted line is the dispersion of the light.

[1] T. Inushima, Phys. Stat. Sol. (c) 4 (2007) 660.

Solid State Spectroscopy of Proteins in Terahertz Region

X. Jin¹, S. Kimura², H. Kihara¹

¹*Department of Physics, Kansai Medical University, 18-89 Uyama-Higashi, Hirakata 573-1136, Japan*

²*UVSOR, Institute for Molecule Science, and School of Physical Sciences, The Graduate University for Advanced Studies (SOKENDAI), Myodaiji, Okazaki 444-8585, Japan*

The terahertz (THz) region of the electromagnetic spectrum has energies of approximately 1 - 10 meV, which corresponds approximately to the frequency range of the transition between rotational states of molecules. Due to the strong frequency-dependent attenuation of water, dry, or partially hydrated samples should be used in the THz study. THz spectroscopy has been used to studying the dynamics of DNA, polypeptide and proteins. [1,2] In order to investigate effects of secondary structures on THz spectra of proteins, we measured the THz spectra of representative proteins having various secondary structures, myoglobin (α -helix-rich), lysozyme (α/β protein), β -lactoglobulin (β -sheet-rich) and α -synuclein (unfolded).

All experiments were done at THz beam line BL6B at UVSOR-II. The thickness of the samples was around 0.5 mm. The lyophilized samples were tightly pressed to form a tablet. The measurements were done at the wavenumber range of 10-200 cm^{-1} at room temperature. Each spectrum was accumulated 500 times. The final spectra were divided by the cell spectrum in order to subtract absorbance of the cell. All measurements were repeated three times to get good consistency. When the wavenumber is above 100 cm^{-1} , absorbance of the protein become very high and noisy.

Figures 1-4 show these protein absorbance spectra. The red lines are smoothed ones. Figures 1 (myoglobin) and 2 (lysozyme) show a broad peak around 20-25 cm^{-1} , respectively, while Figures 3 (β -lactoglobulin) and 4 (α -synuclein) do not show specific peaks at the corresponding region. These results seem to imply that proteins are classified into two different groups, with and without α -helix. It would be more related to the over-all concerted motion of the proteins.

[1] B. Brooks and M. Karplus, Proc. Natl. Acad. Sci. **80** (1983) 6571.

[2] F. P. David *et al.*, Chem. Phys. Chem. **8** (2007) 2412.

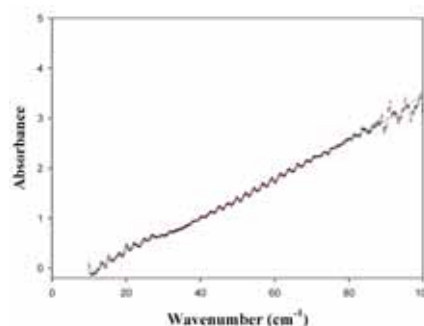


Fig. 1. Absorbance spectrum of myoglobin.

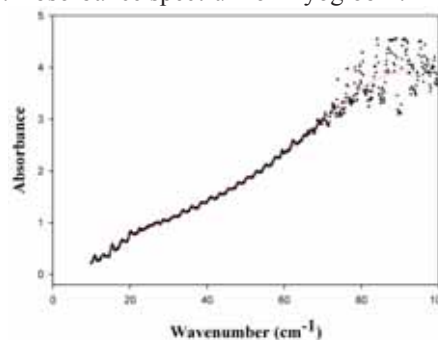


Fig. 2. Absorbance spectrum of lysozyme.

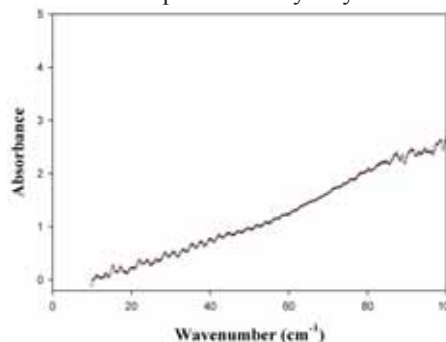


Fig. 3. Absorbance spectrum of β -lactoglobulin.

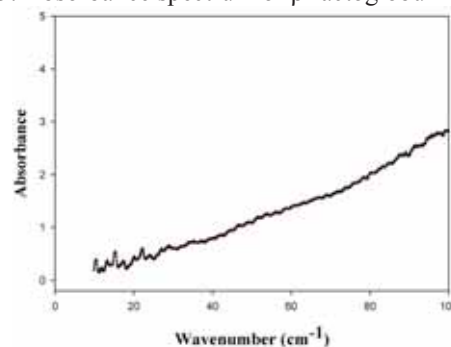


Fig. 4. Absorbance spectrum of α -synuclein

Temperature Dependence of Electron Mobility of InN

R. Ueda, K.Kurihara, T. Yanagawa, K. Fukui, A. Yamamoto
 Dept. Elec. Elec. Engi., Univ. of Fukui, Fukui, 910-8507, Japan

III-V nitride semiconductors and their mixed crystal semiconductors are used for promising high intensity light emitting diodes (LED) and laser diodes (LD). Especially, InN has a matched band gap for the fiber communication wavelength, and it also has small effective mass and high electron mobility which are required for high speed electronic devices. Since, it is difficult to grow bulk InN crystals, the high quality crystalline InN thin films have been fabricated by the MBE or MOCVD methods. However, there is considerable lattice mismatch between InN layer and the substrate (normally Al_2O_3). Then, the electric properties of the InN sample are sometime affected by this interface layer and it is difficult to separate the electric properties of InN crystalline layer from those of the interface layer. Then, the infrared (IR) reflectance measurements have been investigated as one of the complementary measurement methods for obtaining the carrier concentration of the InN crystalline layer. In this method, since the dielectric constant is described by the phonons and plasmon which are characterized by each layer, the reflectance spectra are analyzed by the fitting calculations based on the appropriate layer model [1]. In this report, we extend the aim of those analyses to the electron mobility and demonstrate that the temperature dependence of the electron mobility can be discussed using the infrared reflectance spectra analyses.

Figure 1 shows the typical reflectance spectrum of the InN thin film at 300K and the fitting curve. The carrier concentration measured by Van der Pauw method is $9.8 \times 10^{18} \text{ cm}^{-3}$. The fitted curve shown in Fig. 1 is based on the two layers model which means no consideration of the interface layer in the optical point of view and in agreement with the observed spectrum. The fitting parameters are $\epsilon_\infty = 8.3$, $\omega_L = 581 \text{ cm}^{-1}$, $\omega_T = 478 \text{ cm}^{-1}$, $\omega_p = 836 \text{ cm}^{-1}$, $\gamma = 265$, $\Gamma = 2$ and h (thickness of crystalline InN layer) = 200 nm. Since the effective mass is still unknown for InN, we suppose it is $0.1m_0 \sim 0.15m_0$ according to the theoretical prediction, where m_0 is the static mass of the electron. The carrier concentration derived from IR reflectance spectrum is estimated to $6.5 \sim 9.7 \times 10^{18} \text{ cm}^{-3}$, which is a little smaller than Van der Pauw result. However, from this result, it is concluded that the electric properties of this InN sample are not affected by those of the interface layer.

The γ are described by Eq. (1),

$$\gamma = \frac{e}{m^* \mu} \quad (1)$$

where m^* , n and μ are effective mass, carrier concentration, and electron mobility of the carriers,

respectively. From Eq. (1), the electron mobility can be derived from the IR reflectance measurement by using the damping factor γ of the plasmon which is one of the parameters of the spectrum fitting and the effective mass m^* . Figure 2 shows the electron mobility of the InN crystalline layer derived from the IR reflectance measurements as a function of the temperature. The electron mobility of InN is almost constant in the whole temperature range, and is in agreement with the results of the Hall effect measurement. Therefore, the infrared reflectance spectra analyses can be used for the electron mobility estimation of InN thin films.

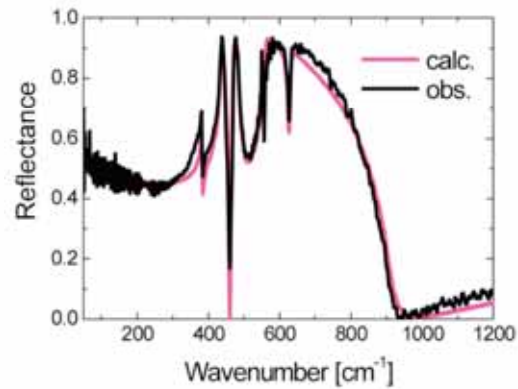


Fig. 1. Reflection spectrum and the fitting result of the InN film in 300K.

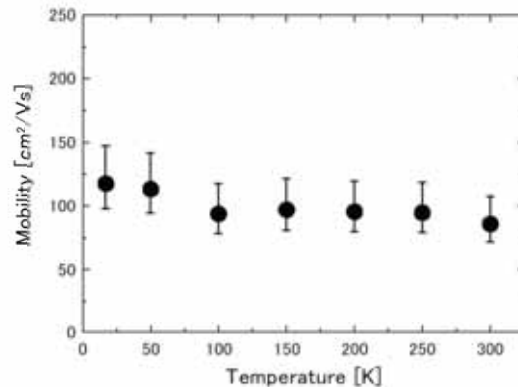


Fig. 2. The electron mobility of the InN crystalline layer at each temperature.

[1] Y. Ishitani *et al.*, *phys. stat. sol. (c)* **0** (2003) 2838.

Comparative Study of Photoluminescence Properties between $\text{ScPO}_4:\text{Zr}^{4+},\text{Mn}^{2+}$ and $\text{YPO}_4:\text{Zr}^{4+},\text{Mn}^{2+}$ Phosphors

Y. Inada¹, M. Kitaura², K. Fukui¹

¹Dep. of Elec. Eng., Univ. of Fukui, Fukui, 910-8507

²Fukui National College Technology, Sabae, 916-8507

Photoluminescence (PL) properties of divalent manganese ions are sensitive for the structure of host crystals. An adjustment of the environment around Mn^{2+} ions by the choice of host materials leads to the improvement of PL properties; the diversification of emission color and the increase in PL intensity. It is thus expected that Mn^{2+} activated phosphors have the potential controlling PL properties artificially on demand. In the present study, we have synthesized the phosphor of $\text{ScPO}_4:\text{Zr}^{4+},\text{Mn}^{2+}$, and the PL and PL excitation (PLE) spectra of it have been measured using vacuum ultraviolet photons.

Samples of $\text{ScPO}_4:\text{Zr}^{4+},\text{Mn}^{2+}$ were synthesized by the solid state reaction with the reagent of Sc_2O_3 , $(\text{NH}_4)_2\text{HPO}_4$, ZrO_2 , and MnC_2O_4 . The concentration of Mn^{2+} and Zr^{4+} ions were adjusted to be 2.5 mol% in preparation. The powders were mixed by a ball mill, and then fired at 800°C in air for 5 hours. The powders thus obtained were sintered at 1200°C in nitrogen atmosphere for 3 hours.

The PL spectrum of $\text{ScPO}_4:\text{Zr}^{4+},\text{Mn}^{2+}$ at 14 K is shown in Fig. 1. In this figure, the PL spectrum of $\text{YPO}_4:\text{Zr}^{4+},\text{Mn}^{2+}$ at 14 K was also shown as a reference. These spectra were obtained under excitation with 6.5 eV photons. The PL spectra of $\text{ScPO}_4:\text{Zr}^{4+},\text{Mn}^{2+}$ and $\text{YPO}_4:\text{Zr}^{4+},\text{Mn}^{2+}$ are dominated by the 2.34 eV (green) band and the 2.53 eV (blue-green) bands, respectively. The PL intensity of the G band is about twice as large as the intensity of the BG band. The PLE spectra for the G and BG bands at 14 K are shown in Figs. 2(a) and 2(b), respectively. The lowest energy peak is located at 3.08 eV in $\text{ScPO}_4:\text{Zr}^{4+},\text{Mn}^{2+}$ and at 3.15 eV in $\text{YPO}_4:\text{Zr}^{4+},\text{Mn}^{2+}$. The peak energy is lower in $\text{ScPO}_4:\text{Zr}^{4+},\text{Mn}^{2+}$ than in $\text{YPO}_4:\text{Zr}^{4+},\text{Mn}^{2+}$.

In the PL and PLE spectra, the G band of $\text{ScPO}_4:\text{Zr}^{4+},\text{Mn}^{2+}$ is similar to the BG band of $\text{YPO}_4:\text{Zr}^{4+},\text{Mn}^{2+}$. As generally accepted, the PL band of Mn^{2+} originates from the transition from the ${}^6\text{A}_1$ (${}^6\text{S}$) ground state to the ${}^4\text{T}_1$ (${}^4\text{G}$) excited state. The energies of the lowest PLE peaks in Figs. 2(a) and 2(b) are close to the energy difference between the ${}^6\text{S}$ and ${}^4\text{G}$ states [1]. This indicates that the G and BG bands originate from the intra-3d transition of Mn^{2+} ions.

As the host material is changed from YPO_4 to ScPO_4 , the lowest PLE peak slightly shifts into low-energy side. Since the ${}^6\text{A}_1 \rightarrow {}^4\text{A}_1 + {}^4\text{E}$ transition is scarcely influenced by the crystal field potential [2],

the peak shift is not due to the change in crystal field strength at the Mn^{2+} site. One plausible effect for the peak shift is the change in electrostatic interaction of 3d electrons in Mn^{2+} ions. In fact, the results in electron spin resonance (ESR) measurement has revealed that the 3d wave function of Mn^{2+} spreads out in ScPO_4 lattice more than in YPO_4 lattice.

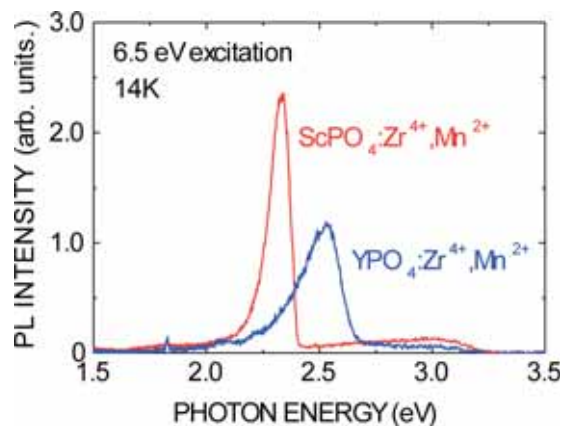


Fig. 1. PL spectra of $\text{ScPO}_4:\text{Zr}^{4+},\text{Mn}^{2+}$ (red) and $\text{YPO}_4:\text{Zr}^{4+},\text{Mn}^{2+}$ (blue) at 14K under excitation with photons at 6.5eV.

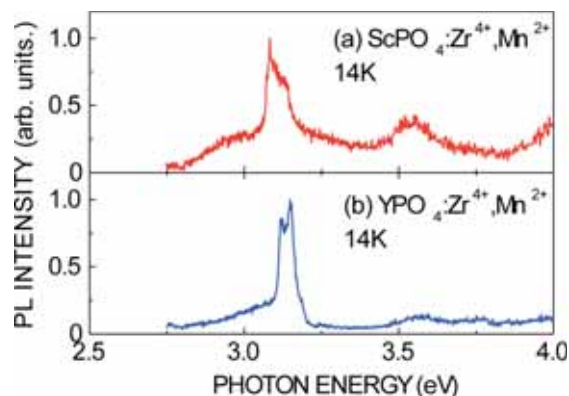


Fig. 2. PLE spectra for the G band in $\text{ScPO}_4:\text{Zr}^{4+},\text{Mn}^{2+}$ (a) and the BG band in $\text{YPO}_4:\text{Zr}^{4+},\text{Mn}^{2+}$ (b) at 14K. The intensities are normalized to unity at their maxima.

[1] J. W. Stout, J. Chem. Phys. **31** (1959) 709.

[2] H. Kamimura, S. Sugano, Y. Tanabe, *Haiishiba Riron to Sono Oyo* (Ligand Field Theory and its Applications) (Shokabo, Tokyo, 1990) 10th ed., 224 (in Japanese).

VUV Reflection Spectroscopy of PdO and PtO Thin Films

Y. Iwai, K. Nakagawa, T. Mizunuma, K. Nakatsuru, K. Chijiwa, K. Ohba, S. Matsumoto, H. Matsumoto

School of Science & Technology, Meiji University, Kawasaki 214-8571 Japan

Both PdO and PtO have the tetragonal cooperite structure (space group D_{4h}^9) and extremely near lattice constants. Extensive experimental and theoretical studies have been performed on the electronic structures of PdO [1, 2]. On the other hand, there are a few reports of PtO in experimental data obtained by electric and optical measurements. To discuss the electronic structures, researchers have tried calculation and referred them [3]. However, because of restricted experimental data, there are unresolved problems such as a behavior like a p-type semiconductor with high conductivity, and an absence of optical band gap.

The purpose of this work was to achieve optical responses of PdO and PtO thin films in wide-range photon energy, and investigate electronic structures by comparing experiment data and theoretical calculation.

Thin films of PdO and PtO were deposited by RF reactive sputtering on fused quartz, at a temperature of 573 °C. Metal palladium and platinum plate were used as the target, and the sputtering was carried out in argon and oxygen mixture gases. The film thickness was about 150 nm. Composition ratio, chemical bonding states and crystallinity of the films were investigated by RBS, XPS and XRD.

Reflection spectra of the films were measured in the vacuum ultraviolet region up to 30 eV with the 3-m normal incident monochromator (grating: G1 and G2) at BL-7B of UVSOR-II. And a silicon photodiode sensor was used as a detector for the reflection light.

According to the analyses, both palladium and platinum oxide thin films are composed of polycrystalline PdO or PtO.

Figure 1 shows the reflection spectra of PdO and PtO thin films at room temperature. Similar characters are involved in each spectrum: a dip named dip-A in the figure located at about 11 eV, a band named band-B at about 6-8 eV in lower energy side of the dip-A, and a broad band with some features above the dip-A. However, these are at different position in energy.

To analyze the differences, DV-X α molecular orbital calculation was performed. Figure 2 shows energy level diagrams of $[M_{13}O_{28}]^{-30}$ (M=Pd, Pt) clusters embedded in Madelung potential represented by formal charges. Band gap arises from the splitting off in the d orbital slightly hybridized with O2p. In each oxide, lower side of d band and O2p band construct the valence band. The reason that the lower

side of valence band lies slightly lower in PtO is considered stronger d-O2p hybridization due to the larger radius of Pt. And now, energy position of the dip-A observed in reflection spectra is higher in PtO thin film. If there is no large difference in unoccupied levels as final states between PdO and PtO, it is consistent with the widths of valence bands and the energy positions of the dips. And on the same assumption, it can be thought that the fact that the band-B is observed at higher energy on PtO originates the downward diffusing of O2p orbital compared to that of PdO.

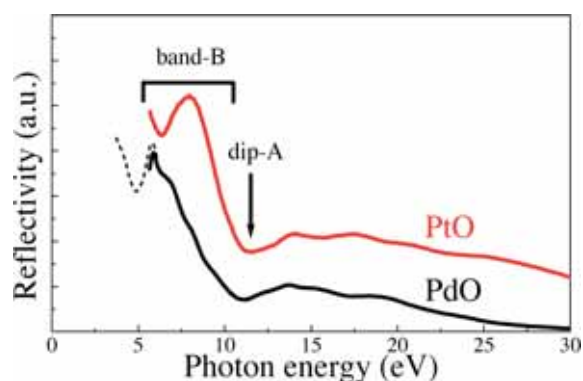


Fig. 1. Reflection spectra of PdO and PtO thin films. The solid line is the data obtained at UVSOR, and the dotted line represents the data obtained elsewhere.

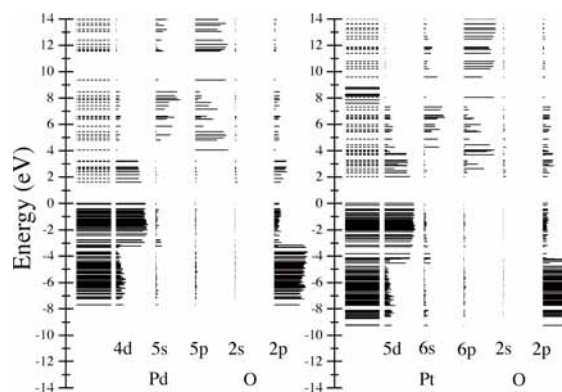


Fig. 2. Energy level diagrams of $[M_{13}O_{28}]^{-30}$ cluster (M=Pd, Pt). The energy is referred to the top of the valence band. The broken lines represent unoccupied levels.

[1] H. A. E. Hagelin *et al.*, *J. Electron. Spectrosc. Relat. Phenom.* **124** (2002) 1.

[2] R. Ahuja *et al.*, *Phys. Rev. B* **50** (1994) 2128.

[3] J. Uddin *et al.*, *Phys. Rev. B* **71** (2005) 155112.

Angle Dependence of Polarized Excitation Spectra in AlGa_xN

M. Kishida¹, F. Suzuki¹, K. Fukui¹, H. Miyake², K. Hiramatsu²
¹Dept. Elec. Elec. Engi., Univ. of Fukui, Fukui 910-8507, Japan
²Dept. Elec. Elec. Engi. Mie Univ., Mie 514-8507, Japan

AlGa_xN alloys are becoming important optical materials which have the UV emission bands with the variable photon energies from 3.4 to 6.28 eV, therefore the studies of mechanisms of UV emissions require wide energy range of the excitation photons, and the SR is well-suited.

The band structures of both AlN and GaN are shown in Figure 1. The valence band at the Γ point is splitting into three bands by the crystal field effect (Δ_{cr}) and the spin orbit interaction (Δ_{so}). The three bands are called as crystal field split off hole (CH) band, heavy hole (HH) band, and light hole (LH) band, respectively, and the transitions from CH, HH and LH bands to the conduction band are labeled as A, B and C transitions, respectively. Furthermore, since these bands have the anisotropy, the A transition is allowed under $E//c$ condition, and both B and C are $E \perp c$, where E and c represent the electric field vector of the excited light and the crystal axis, respectively. Usually, the AlGa_xN (including GaN and AlN) crystalline thin films become wurtzite structure, and c -axis is perpendicular to the surface. Therefore the minimum band gap excitation is allowed in the case of GaN (B transition), but is not in the case of AlN (A transition). These conditions directly affect to the optical properties, and the experimental research of finding the band inversion Al fraction is important. Then, we have been measured the angle dependent polarized photoluminescence excitation spectra.

Al_xGa_{1-x}N ($x = 0.46, 0.54, 0.65, 0.74, 0.763$) samples were grown on the sapphire substrates via 1 μ m AlN single crystal films by MOVPE method at Mie University. The thicknesses of AlGa_xN thin films are about 1 μ m. All measurements were performed at about 20K.

Figure 2 shows the excitation spectra of Al_{0.763}Ga_{0.237}N at 0 degree of the incidence angle ($E \perp c$) and 60 degree. The $E // c$ spectra is calculated using these two spectra. The intensity of the $E // c$ spectrum is higher than that of the $E \perp c$, and the red shift of the peak energy is observed in the $E \perp c$ spectrum. These results represent that the A transition is allowed at $x = 0.763$, Δ_{so} is not clear (small), and the shift represents Δ_{cr} .

Figure 3 shows the Al fraction dependence of Δ_{cr} . The Δ_{cr} s at $x = 0$ and 1 are taken from ref. 1. Fig. 3 results shows the band inversion is occurred at around $x = 0.5$. Fig. 3 also indicates that there is the negative bowing which is similar to the x dependence of the band gap itself, though the bowing parameters are different with each other.

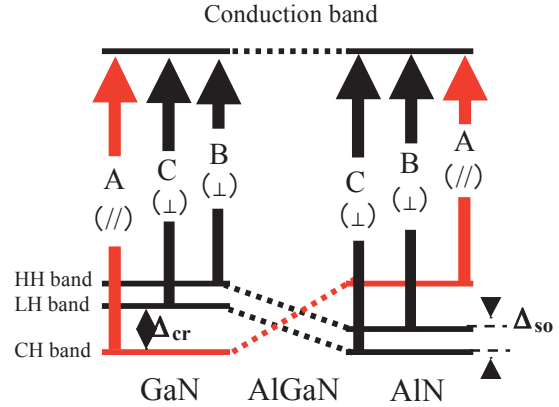


Fig. 1. Band structures of AlN, GaN and AlGa_xN.

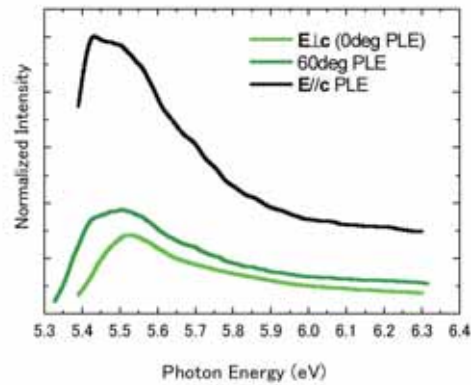


Fig. 2. Angle dependence of the polarized photoluminescence excitation spectra (PLE) of Al_{0.763}Ga_{0.237}N.

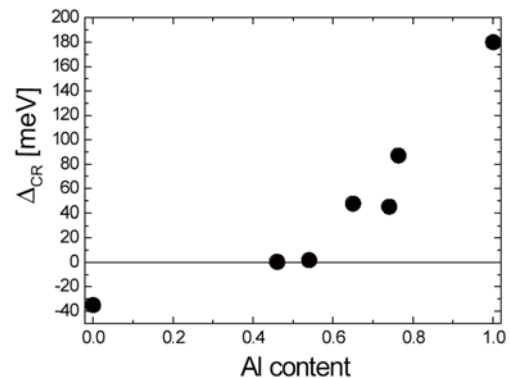


Fig. 3. Al fraction dependence of Δ_{cr} .

[1] A. Shikanai *et al.*, J. Appl. Phys, **81** (1997) 417.

Temperature Dependence of the Photoluminescence of the SrScCuOS Layered Oxysulfide

T. Nakazato¹, Y. Furukawa¹, H. Ogino², S. Saito¹, S. Ono³, N. Sarukura¹, K. Kishio²

¹*Institute of Laser Engineering, Osaka University, Osaka 565-0871 Japan*

²*Department of Applied Chemistry, University of Tokyo, Tokyo 113-8656, Japan*

³*Faculty of Engineering, Nagoya Institute of Technology, Nagoya 466-8555, Japan*

The development and engineering of the wide gap semiconductors are important for optoelectronics. Electrical and optical properties of various III-V or II-V compounds have become clear that the photoabsorption and the emission near the band gap are dominated by excitons. It is said that the excitons enhance emission efficiency because of their large oscillator strengths and room temperature excitonic emission is crucial for light emitting diode operation. Unfortunately, excitons are usually only experimentally observed in high quality crystals and at low temperatures. Ueda *et al.*[1], investigated the temperature dependence of the photoluminescence (PL) spectra of LaCuOS and found that the emission from excitons can be observed at room temperature. They also mentioned that the Cu-S bonding in Cu-S layer defines the electronic structures near band gap. We are interested in SrScCuOS because it has Cu-S layer as LaCuOS. This suggests that it could also be a potential UV material. In the present study, we have measured the temperature dependence of the PL spectra of SrScCuOS to evaluate the optical properties.

We have measured the PL spectra of 3 SrScCuOS crystals, labeled sample A, B, C and E at the BL7B port of the UVSOR. The excitation wavelength was 340 nm. In order to investigate the temperature dependence of PL spectra, these measurements have been carried out at 24-120 K and room temperature.

Figure 1 shows the temperature dependence of the PL spectra. The peaks exist at about 370 nm in all samples. The peak intensities become stronger with lower temperature. These spectra have interesting temperature dependence as will be discussed below. In the case of sample A and E, only one broad peak was found for each temperature setting. A blue shift is observed and the width becomes narrower at lower temperature. Samples B and C showed not only a narrowing of the peak width but a splitting was observed, as well. A temperature dependent relative blue shift between the two peaks could not be observed due to limitations in the spectral resolution. The shorter wavelength peak relatively becomes stronger as compared with the longer wavelength feature as temperature is increased in both samples, B and C. At present, we cannot conclude whether these peaks in each sample are excitonic in nature. Nonetheless, the prospects are interesting because excitonic emission in oxides has not been reported so often. The differences in the PL spectra of A, B, C and E might originate from anisotropy in the defects, impurities, or structures of the Cu-S layers.

We have measured the temperature dependence of

the PL spectra of SrScCuOS to evaluate the optical properties. An intensive temperature-dependent PL and absorption study is necessary to confirm the excitonic nature of the observed UV emission.

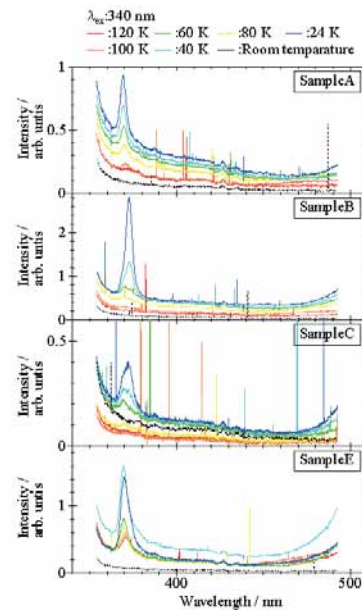


Fig. 1. PL spectra of the SrScCuOS at 20-120 K and room temperature. The excitation wavelength is 340 nm.

[1] Ueda *et al.*, Appl. Phys. Lett. **78** (2001) 2333.

Energy and Temperature Dependences of Time Resolved Decay Curves in AlGa_xN Alloys

T. Sakai¹, M. Suzuki¹, T. Kondo¹, K. Fukui¹, S. Naoe², H. Miyake³, K. Hiramatsu³

¹Dept. Elec. Elec. Engi., Univ. of Fukui, Fukui 910-8507, Japan

²Dept. Mech. Sys. Engi., Kanazawa Univ., Kakuma, Kanazawa 920-1192, Japan

³Dept. Elec. Elec. Engi., Mie Univ., Mie 514-8507, Japan

The ternary AlGa_xN alloys are promising materials for ultraviolet (UV) optical devices. They are known as the wide band gap semiconductors with the features of the high melting point and the high hardness. The mechanisms of the near band edge photoluminescence (PL) are not clarified enough though the qualitative improvements of the AlGa_xN emission devices are remarkable. We have been measuring PL, PL excitation (PLE) and time resolved decay (TRD) curves. These results suggest that the near band edge emission band consists of three adjacent emission components (bands) which interact with each other, especially lower two components show the highly efficient energy transfer between them. In this experiment, we have been carried out both the energy and temperature dependence TRD curves of the various Al fraction samples to confirm this model.

Al_xGa_{1-x}N ($x=0.37\sim 0.85$) samples were made by the MOVPE method at Mie University. The thicknesses of AlGa_xN thin films are about 1 μ m on 1 μ m AlN single crystal films with Al₂O₃ substrates. The TRD measurements were performed at single bunch operation modes. A conventional 30cm VIS-UV monochromator with liquid N₂ cooled CCD detector is used for PL measurements of all samples. The time region of our TRD measurements using TAC method (time correlated single photon counting method) is 0~178 ns and the resolution is about 1 ns.

Figure 1 shows PL spectra of the three adjacent components and the total of various Al fraction samples at ~10K. Three components are called as the slow (in the order of 100 ns or less), middle (10 ns order), and fast (less than 1 ns : under the time resolution of our TAC system). The total spectrum represents the sum spectrum of these three components, and it must be in good agreement with the normal (time integrated) PL spectra, conversely, the agreements between the total spectra in Fig. 1 and the normal PL spectra of the various Al fraction samples are good validation checks of our model. In fig.1, it is quite obvious that the slow component become dominant with increasing Al fraction. This behavior is similar to the Al fraction dependence of the PL band width. Since the PL band width corresponds to the classical alloy broadening, the compositional inhomogeneity is increasing with increasing Al fraction up to $x = 0.85$ and probably introduces some kinds of defects.

Figure 2 shows the temperature dependences of

three components of Al_{0.54}Ga_{0.46}N. The hot colors represent the high intensity regions. The intensity alternation from slow component to middle one with increasing temperature is clearly seen at the low temperature, and similar behavior is also seen between middle to fast at higher temperature side. The intensity alternation between slow and middle components reveals that there is the energy transfer path between them and the thermal energy makes the excited electrons at the energy level corresponded to the slow component move to that corresponded to the middle component. These kinds of the intensity alternations are seen in all Al fraction samples, and we think we can confirm our model at the various Al fraction samples.

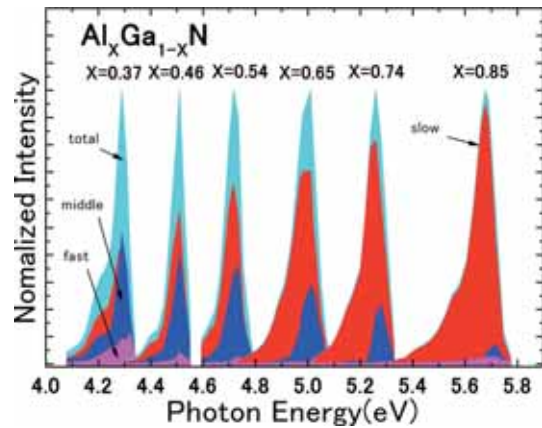


Fig. 1. PL spectra of each element in all samples.

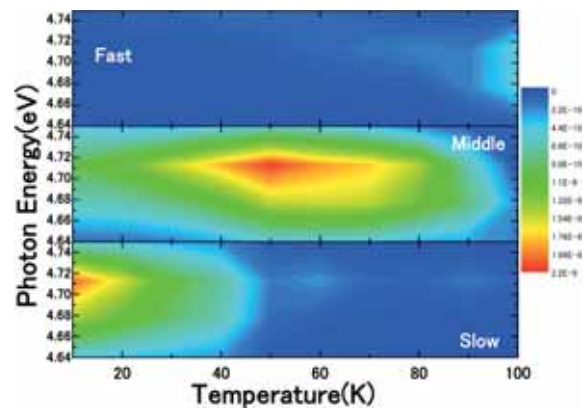


Fig. 2. Temperature dependence of time resolved PL spectra of Al_{0.54}Ga_{0.46}N.

BL7B Photoabsorption Cross Section of C₆₀ Thin Film from 1.3 to 42 eV

H. Yagi¹, K. Nakajima², K. R. Koswattage³, K. Nakagawa³, C. Huang¹,
Md. S. I. Proadhan¹, B. P. Kafle¹, H. Katayanagi¹, K. Mitsuke¹

¹Department of Photo-molecular Science, and Grad. Univ. Adv. Studies,
Institute for Molecular Science, Okazaki 444-8585, Japan

²Science Research Center, Hosei University, Chiyoda-ku, Tokyo 102-8160, Japan

³Faculty of Human Development, Kobe University, Nada-ku, Kobe 657-8501, Japan

Since the discovery of the method for bulk synthesis of C₆₀ [1], optical properties of solid C₆₀ have been studied by various techniques. But most of the studies were restricted to photon energies below 7 eV. Above 11 eV, only EELS measurements were carried out. In the present study, we have measured absorption spectra of C₆₀ thin films from 1.3 eV to 42 eV.

C₆₀ films were prepared by vacuum deposition on collodion thin film substrates. The deposition rate and the amount of deposited C₆₀ were estimated from the readings of the crystal-oscillator surface thickness monitor (Inficon, XTM/2). Collodion substrates and the thickness monitor were located 90 mm above the sample holder and at symmetrical positions with respect to the molecular beam axis. We prepared three samples with the thickness $d = 11, 28,$ and 57 nm. The deposition rate was $0.16\text{-}0.29$ Å/s. Optical absorption measurements were carried out at BL7B of the UVSOR facility. The photoabsorption cross section of C₆₀ film was estimated by using the Lambert-Beer law

$$I = I_0 \exp(-\sigma N d) \quad (1)$$

Here, σ is the photoabsorption cross section, N is the number density of C₆₀ molecules and calculated from the mass density 1.65 g/cm³ [2], d is the C₆₀ film thickness, I_0 is the light intensity after passing through a substrate, and I is the light intensity after passing through a C₆₀ film and a substrate. I_0 and I were measured successively and normalized by the ring current in the storage ring.

The σ values obtained from the results of 28 and 57 nm thick films show good agreement at $h\nu \leq 12.5$ eV. In the energy range 12.5-27.5 eV, I was so small for the 57 nm thick film that we could not estimate correct σ values. The σ from the results of 11 nm thick film also shows good agreement with those of the other films if multiplied by a factor of 0.85. This is probably due to the uncertainty of the film thickness of 11 nm thick film. Figure 1 shows thus estimated photoabsorption cross section of C₆₀ thin film (black curve) in comparison with that calculated from EELS spectra of C₆₀ thin film (green curve) [3]. The two curves are almost consistent with each other. Photoabsorption cross section of gaseous C₆₀ is also shown in Fig. 1 (red curve) [4]. The positions of the peaks and shoulders on the σ curve for the C₆₀ thin film agree well above 10 eV with those for gaseous C₆₀. This agreement, however, becomes worse below

7 eV and the width of the peak at 22 eV is much larger in the solid phase.

Smith has shown that absorption spectra of C₆₀ in the gas phase and solution resemble each other [5] by introducing the Chako factor [6]

$$\alpha_s/\alpha_g = (n^2+2)^2/9n \quad (2)$$

Here, α_s and α_g are the absorption coefficient in solution and in the gas phase, respectively, and n is the refractive index of the solution. Linder shows that when the solvent is not transparent, Chako factor should be replaced by [7]

$$\alpha_s/\alpha_g = [(n^2+2-k^2)^2+(2nk)^2]/9n \quad (3)$$

Here, k is the extinction coefficient of the solution. These factors are derived by considering the effect of van der Waals interaction and Lorentz local field. Solid C₆₀ is a molecular solid which is bonded by weak van der Waals forces with a cubic structure. Therefore this relation is probably applicable to the solid C₆₀. Present data multiplied by the the Linder factor is shown in Fig. 1 (blue curve). Here, n and k are calculated from the EELS spectra [3]. After the correction of the Linder factor, the present data agrees very well with σ in the gas phase except in the energy range 24-34 eV.

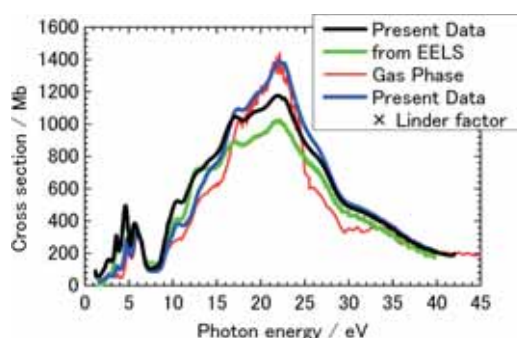


Fig. 1. Photoabsorption cross section of C₆₀.

- [1] W. Kratschmer *et al.*, Nature **347** (1990) 354.
- [2] K. Prassides, H. W. Kroto, Phys. World **5** (1992) 44.
- [3] E. Sohmen *et al.*, Z. Phys. B Condens. Matter **86** (1992) 87.
- [4] B. P. Kafle *et al.*, J. Phys. Soc. Jpn **77** (2008) 014302.
- [5] A. L. Smith, J. Phys. B **29** (1996) 4975.
- [6] N. Q. Chako, J. Chem. Phys. **2** (1934) 644.
- [7] B. Linder and S. Abdunur, J. Chem. Phys. **54** (1971) 1807.

BL7B Photoabsorption Cross Section of C₇₀ Thin Film from 1.3 to 39 eV

H. Yagi¹, K. Nakajima², K. R. Koswattage³, K. Nakagawa³, C. Huang¹,
Md. S. I. Proadhan¹, B. P. Kafle¹, H. Katayanagi¹, K. Mitsuke¹

¹Department of Photo-molecular Science, and Grad. Univ. Adv. Studies,
Institute for Molecular Science, Okazaki 444-8585, Japan

²Science Research Center, Hosei University, Chiyoda-ku, Tokyo 102-8160, Japan

³Faculty of Human Development, Kobe University, Nada-ku, Kobe 657-8501, Japan

The optical properties of solid C₇₀, the second most stable and abundant fullerene, have been studied by a variety of techniques, though most of the studies were restricted to photon energies below 6 eV. Even in this energy range, the values of the photoabsorption cross section of solid C₇₀ differ between different literature. In the present study, we have measured the absorption spectra of C₇₀ thin films from $h\nu = 1.3$ eV to 39 eV.

In the vacuum, C₇₀ films were deposited on collodion thin film substrates. The details of sample preparation are described elsewhere [1]. We prepared three samples with the thicknesses of $d = 11$, 29, and 57 nm. The deposition rate ranges between 0.19-0.26 Å/s. Optical absorption measurements were carried out at BL7B of the UVSOR facility. The photoabsorption cross section of the C₇₀ film was estimated by using the Lambert-Beer law

$$I = I_0 \exp(-\sigma Nd). \quad (1)$$

Here, σ is the photoabsorption cross section, N is the number density of C₇₀ molecules and calculated from the mass density 1.64 g/cm³ [2], d is the thickness of the C₇₀ film, I_0 and I are the intensities of the light measured with a photodiode by inserting, respectively, the film of neat collodion and that of collodion covered with C₇₀ across the photon beam axis. The intensity was measured successively at wavelength intervals of 1 nm and normalized by the storage-ring current.

Figure 1 shows the photoabsorption cross section of the three C₇₀ samples with different thicknesses. Their σ values do not agree with each other. Figure 1 also contains the σ curve calculated from the reported EELS spectra of C₇₀ thin film with the thickness of 200 nm (green curve) [3]. Our σ curve for the 29 nm C₇₀ film and that calculated from EELS show good agreement at $h\nu \geq 25$ eV. Figure 2 shows the expanded spectra of Fig. 1 at $h\nu \leq 6$ eV. The σ values determined from EELS [3], ellipsometry [4], and optical absorption spectroscopy [5] are also plotted. These results and our present data are not consistent with each other. This is possibly due to the difference of the crystal structure. At room temperature, solid C₇₀ adopts face-centered cubic (fcc) or hexagonal close packed (hcp) structures depending on the history of its formation [2]. A number of effects determine the relative abundances of hcp and fcc phases. In the present study, the conditions of sample preparation were almost the same for all the samples. Therefore, the thickness of the C₇₀ film may affect the

crystal structure, or there may be other reason for the disagreement between the three σ curves.

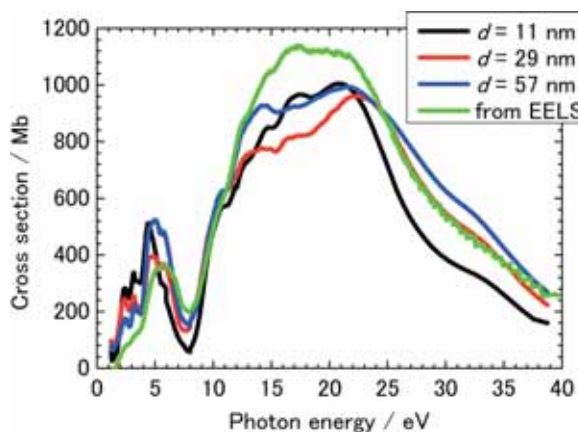


Fig. 1. Photoabsorption cross sections of C₇₀ thin films from 1.3 to 39 eV.

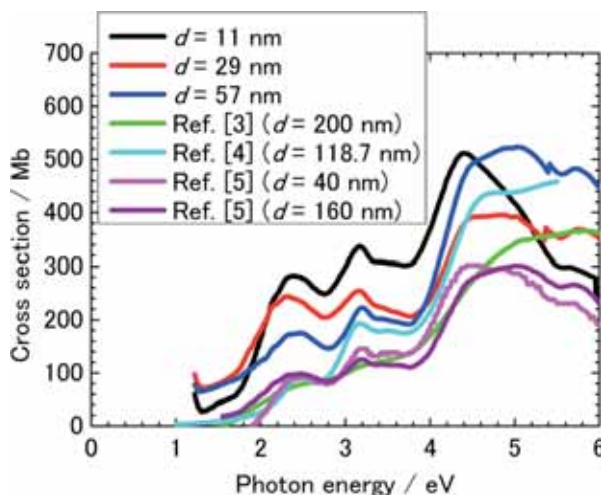


Fig. 2. Photoabsorption cross section of C₇₀ thin films below 6 eV in comparison with those of other studies [3-5].

- [1] H. Yagi *et al.*, UVSOR Activity Report 2007 (2008).
- [2] G. B. M. Vaughan *et al.*, Science **254** (1991) 1350.
- [3] E. Sohmen *et al.*, Z. Phys. B Condens. Matter **86** (1992) 87.
- [4] Ren *et al.*, Appl. Phys. Lett. **61** (1992) 124.
- [5] Zhou *et al.*, J. Appl. Phys. **80** (1996) 459.

Pumped Wavelength-Dependence of Ce:LuLiF₄ as Fast Scintillator Using Storage Ring Free-Electron Lasers

Y. Furukawa¹, T. Nakazato¹, M. Cadatal², M. Pham², T. Tatsumi¹, A. Saiki¹, Y. Arikawa¹, S. Saito¹, N. Sarukura¹, H. Nishimura¹, H. Azechi¹, K. Mima¹, T. Fukuda³, M. Hosaka⁴, M. Katoh⁴, N. Kosugi⁴

¹Osaka university, Yamadaoka2-6, Suita, Osaka565-0871, Japan

²The Graduated University for Advanced Studies, Hayama, Kanagawa 240-0193, Japan

³Tohoku University, 2-1-1 Katahira, Aoba-ku, Sendai 980-8577, Japan

⁴Institute for Molecular Science, Myodaiji, Okazaki, Aichi 444-8585, Japan

There is an emerging demand for the development of fast neutron scintillator for laser confined nuclear fusion with a fast ignition scheme [1]. For the precise measurement of ignition timing, a scintillator with a fast response time to the high-energy neutron while providing sufficient contrast to the gamma ray is still under investigation. Li 6 is known to have a large cross section for high-energy neutrons. Therefore, lithium-rich compounds with high quantum efficiency light emitting ion are the prominent candidates. From this aspects, we have considered Ce:LuLiF₄.

For the development of such scintillation devices, the characterization of the response time for different neutron or photon excitation energies is extremely important for the optimum design of the material and doping concentration.

For this purpose, free electron lasers (FEL) are attractive for their flexible tunability. Among such FELs, storage ring free-electron lasers (SRFEL) should be the appropriate choice because of their adequately high repetition rate [2].

In this presentation, Ce:LuLiF₄ as a fast scintillator is evaluated using a SRFEL operated in deep UV region. The response time is found to remarkably shorten for the excitation of the lower level of the absorption band.

The SRFEL at the UVSOR facility in the Institute for Molecular Science, Japan was used as the excitation light source. The excitation wavelengths used are 216 nm and 243 nm. The repetition rate of FEL is 11.3 MHz. The SRFEL was focused on the sample. The fluorescence spectrum and the fluorescence lifetime of the Ce:LuLiF₄ sample are measured using the spectrograph coupled to a streak camera. The two peaks in streak camera image as shown in Fig. 1 are attributed to the 11.3 MHz laser repetition rate. Fig. 2 shows that the fluorescence decay time for excitation wavelengths of 290 nm, 243 nm, and 216 nm are 43 ns, 32 ns, and 35 ns, respectively.

In conclusion, the response time is found to be remarkably shortened for the excitation of lower-level of the absorption band of Ce:LuLiF₄ as fast scintillator. This response time is already

acceptable for the scintillator for the diagnostic device for the laser fusion with fast ignition scheme. The SRFEL operated in deep UV region is shown to be powerful tool for the material survey of neutron scintillation devices.

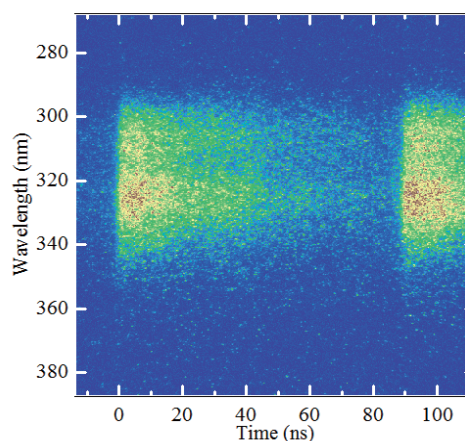


Fig. 1. Streak camera images of Ce:LuLiF₄ emission when excited with 216 nm.

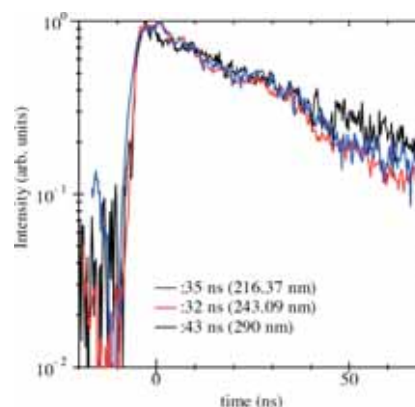


Fig. 2. Fluorescence lifetimes for 290 nm, 243 nm, and 216 nm excitation.

[1] R. Kodama *et al.*, Nature **432** (2004) 1005.

[2] M. Hosaka *et al.*, Nucl. Inst. Methods in Phys. Res. A **483** (2002) 146.